Use of the Ocean Surface Wind Direction Signal in Microwave Radiance Assimilation

Masahiro Kazumori[a*] and Stephen J. English[b]

[a] Japan Meteorological Agency, Tokyo, Japan
[b] European Centre for Medium-Range Weather Forecasts, Reading, UK
[*] Correspondence to: M. Kazumori, 1-3-4 Otemachi, Chiyoda-ku, Tokyo 100-8122, JAPAN
E-mail: kazumori@met.kishou.go.jp

Abstract

We developed an empirical relative wind direction (RWD) model function to represent azimuthal variations of oceanic microwave brightness temperatures of vertical and horizontal polarizations. The RWD model function was based on brightness temperature measurements from the Advanced Microwave Scanning Radiometer and Special Sensor Microwave Imager Sounder (SSMIS). Ocean surface wind vector data from SeaWinds on board the Advanced Earth Observing Satellite – II and European Centre for Medium-Range Weather Forecasts (ECMWF) Integrated Forecasting System were utilized for the RWD model function development. The RWD model function was introduced to a microwave ocean emissivity model; a FAST microwave Emissivity Model (FASTEM) in a radiative transfer model for satellite radiance assimilation. Performances of the RWD model function were much more realistic than present azimuthal model functions in FASTEM for low wind speed and high frequency channels.

An assimilation experiment using the RWD model function was performed in the ECMWF system. The experiment demonstrated reductions of first guess departure biases arising from modelling of the azimuthal variations in areas of high wind speed and low variability of wind direction. For example, bias reductions in ascending and descending SSMIS 19 GHz vertical polarized brightness temperature in Somali jet at the Arabian Sea were approximately 0.6 K and 0.7 K. The bias reductions were found for all assimilated microwave imager channels in a wide wind speed range. Moreover, analysis increments of specific humidity in the lower troposphere were reduced (e.g., 0.3 g kg^{-1} reduction at 1000 hPa in the Somali jet). We found improvements of relative humidity and temperature in short-range forecasts in the lower troposphere. The experiment results clearly showed the importance of modelling the azimuthal variation of emissivity for assimilation of microwave imager observations. The RWD model function should be included in the radiative transfer model used in the microwave radiance assimilation observation operator.

1. Introduction

Microwave radiance data measured from satellites is a crucial data source in data assimilation for numerical weather prediction (NWP). The radiance data are assimilated as brightness temperatures by means of radiative transfer calculations. Oceanic microwave radiance data contain various geophysical information: water vapour, atmospheric hydrometeors and ocean surface conditions. The sensitivity needs to be included in the radiative transfer calculations in order to make consistent changes in the initial state.

The ocean surface properties can be represented with several parameters because the ocean surface is more homogeneous than the land surface. For calm oceans, ocean surface emissivity can be accurately computed using the Fresnel equation by assuming specular surface. The emissivity is expressed as a function of a permittivity, sea surface temperature, and incidence angle. In practice, the ocean surface is rough. The primary cause of the surface roughness is wind. The ocean surface roughness increases the emissivity. Accurate modelling of the ocean surface emissivity is necessary in physically based remote sensing both for geophysical parameter retrievals, and in data assimilation.

Furthermore, the ocean surface radiance observed with microwave radiometers has a wind direction signal. Consequently, vertically and horizontally polarized oceanic microwave radiations have an azimuth angle dependency. The definition of the azimuth angle in this study and relevant angle information are described in the Appendix. In airborne radiometer field experiments during the 1990's, the azimuthal variation was clearly observed (Etkin *et al*., 1991, Dzura *et al*., 1992, Yueh *et al*., 1995, Yueh *et al*., 1997, Yueh *et al*., 1999). The signals vary as a function of the azimuth angle, wind speed, and incidence angle. In theoretical studies on the ocean surface emissivity (Tsang, 1991, Yueh, 1994, Yueh, 1997), their models were able to explain the azimuthal variation in horizontal and vertical polarized brightness temperature, and in the third and fourth Stokes parameters. Moreover, the signal was found in analyses of space-borne radiometer measurements; Special Sensor Microwave/Imager (SSM/I) (Wentz, 1992, Meissner and Wentz, 2002). These experiments and analyses showed that brightness temperatures at 19 and 37 GHz have dependencies on wind direction relative to the sensor viewing angle. In other words, the directional features of ocean surfaces can be measured as the azimuthal variation of the brightness temperatures. In geophysical parameter retrievals (e.g., sea surface temperature, sea surface wind speed and total column water vapour) from the satellite radiance data, the directional signal has been thought as one of the error sources and been removed to obtain accurate the geophysical parameters. Moreover, the signals are actively used as a geophysical model function (GMF) in wind vector retrievals from scatterometers (QuikSCAT, ASCAT) and WindSat measurements.

Wentz (1997) showed that inclusion of the azimuthal variation in a wind speed retrieval algorithm can significantly improve the accuracy of the wind speed product. Meissner and Wentz (2002) proposed an ocean emissivity model for the oceanic geophysical parameter retrievals and recently their model was updated (Meissner and Wentz, 2012). Their latest model has an updated function to express the azimuthal variation in terms of a relative wind direction. The relative wind direction (RWD) is a wind direction relative to the satellite azimuth angle. Their model function was developed based on a collocated data set of brightness temperature measurement from WindSat, and SSM/I, and wind observations from QuikSCAT.

In radiance data assimilation communities, a FAST microwave Emissivity Model (FASTEM) was developed (English and Hewison, 1998) for radiative transfer models; RTTOV (Saunders *et al*., 1999) and CRTM (Weng *et al*., 2005). FASTEM is a semi empirical model and has been widely used

in many operational NWP centres, with the aim of computationally fast and accurate results. The initial version of FASTEM (FASTEM-1) was based on a geometric optics (GO) model simulation results. An updated version, FASTEM-2, by Deblonde and English (2001) was released in RTTOV-7 (Saunders *et al*., 2002). An azimuthal variation model function was introduced for the first time in FASTEM-3 (Liu and Weng, 2003), released as part of RTTOV-8 (Saunders *et al*., 2006). In FASTEM-4 (Liu *et al*., 2011), an updated permittivity calculation, a new parameterizations of the roughness effect, foam parameterization and a new azimuthal model function were introduced. FASTEM-5, again modified the large scale roughness and foam parameterization. FASTEM-4 and -5 are incorporated in RTTOV-10 (Saunders *et al*., 2012) and RTTOV-11 (Saunders *et al*., 2013). The impact of FASTEM-4 and FASTEM-5 for NWP was evaluated at the European Centre for Medium-Range Weather Forecasts (ECMWF) and FASTEM-5 was selected for operational use (Bormann *et al*., 2011, Bormann *et al*., 2012).

However, the azimuthal model function in FASTEM-3, -4 and FASTEM-5 have not been used for microwave imagers in the operational NWP centres because the sensor azimuth angle information is not always available in real time radiance data and insufficient modelling of the azimuthal variation in the emissivity model. The FASTEM-5 azimuthal model function is employed for microwave sounding instruments (e.g., Advanced Microwave Sounding Unit - A (AMSU-A), Microwave Humidity Sounder (MHS)) in the ECMWF system. However, because surface sensitive window channels in the microwave sounding instruments (e.g., AMSU-A channel 1, 2, 3, and 4, MHS channel 1 and 2) are not actively assimilated (only used for quality-controlling the lower tropospheric channels), it is thought that the azimuthal variation of the surface emissivity in microwave sounding data has a minor effect on the data assimilation.

Furthermore, other biases in simulated radiance had been thought to be much larger than those from the surface wind direction signal. Therefore, the importance of the azimuthal variation in the microwave imager measurements was thought to be negligible (Bormann *et al*., 2011) and has been overlooked in the radiance assimilation communities. No investigations focussed on the effect of the azimuthal variation in the microwave radiance assimilation have been performed so far.

As shown in the literature on geophysical retrievals, the azimuthal variation reaches about 2 K in high wind speed conditions. The phenomena should be taken into account correctly in the calculation of microwave ocean emissivity for the radiance assimilation. Otherwise, the signals of the azimuthal variation may cause incorrect increments or excessive data rejection in the data assimilation, especially under strong wind conditions. Furthermore, the short range forecast accuracy has increased significantly in recent years, so errors arising from the neglect of an azimuthal model function in the radiative transfer model are increasingly significant.

The goal of this study is to investigate the impact of the wind directional signal in the microwave radiance assimilation. To achieve this, the missing sensor azimuth angle in the real time data are calculated based on satellite sensor locations and scan geometry for The Tropical Rainfall Measuring Mission (TRMM) Microwave Imager (TMI) and Special Sensor Microwave Imager Sounder (SSMIS). We developed a new relative wind direction (RWD) model function to express the azimuthal variation for the microwave radiance assimilation. The RWD model function was compared with present model functions in FASTEM-5 and FASTEM-3. And we performed a data assimilation experiment using the RWD model function to examine its scientific impacts.

In section 2, we describe the microwave ocean emissivity models, the derivation of the RWD model function and their comparison results. In section 3, the impact study and the experimental results are given. In section 4, we discuss our results and provide our conclusion.

2. Modelling of microwave ocean surface emissivity

2.1 Design of model

A calm ocean surface is characterized by a polarized emission. The emissivity can be calculated assuming specular reflection using the Fresnel equation (Liou, 2002). The emissivity is a function of frequency, polarization, incidence angle, sea surface temperature, and salinity. When the surface is roughened by wind, the roughness of the surface increases the emissivity. In the modelling of microwave ocean emissivity, the roughness scales can be modelled with two scales. One is large scale roughness; i.e., gravity waves or swell whose wavelengths are large compared with the microwave radiation wavelength. The other is small scale roughness; i.e., capillary waves whose wavelengths are small compared with the microwave radiation wavelength. The small scale waves can be considered a modulation of the large scale wave. Furthermore, the breaking waves produce foam and whitecap. They increase the emissivity because the foam and whitecap behave like a blackbody in the microwave frequency range.

These three contributions (1. large scale roughness, 2. small scale roughness, and 3. foam and whitecap) are parameterized and have been updated in the development of FASTEM.

1) Large scale roughness effect

This phenomenon can be modelled as an ensemble of tilted facets, and each facet can be thought as independent specular surface. In FASTEM, this contribution is integrated and parameterized as a function of incident angle, wind speed and frequency to achieve the computational fast performance. FASTEM-1 parameterized the large scale roughness effect based on a geometric optics (GO) model output. FASTEM-2 added a correction term to the reflectivity by using surface-to-space transmittance and updated the parameterization coefficients based on GO model. The emissions from the large scale wave are assumed to be isotropic in azimuthal direction.

2) Small scale roughness effect

The roughness effect from the small scale wave is a source of Bragg scattering and diffraction at the microwave frequency range. The small scale roughness effect also increases the emission. FASTEM-1 added an empirically derived correction factor (an exponential function of incidence angle) to the reflectivity. FASTEM-4 introduced an improvement to the roughness parameterization based on a two-scale emissivity model. Although the Bragg scattering by small scale waves is the dominant effect in the directional signals (Yueh, 1997), there is no azimuthal dependence model function on the small scale roughness effect in the FASTEM because the surface spectrum was assumed to be isotropic.

3) Foam and whitecap

In FASTEM-1, 2 and 3, foam cover is modelled as a function of 10 m wind speed (Monahan and O'Muircheartaigh, 1986). Although FASTEM-4 introduced Tang (1974) foam cover parameterization, the model was reverted from Tang (1974) to Monahan and O'Muircheartaigh (1986) in FASTEM-5. The foam functions are parameterized based on 10 m wind speed.

In addition to these three effects in FASTEM, a correction model to allow for the azimuthal variation of the emissivity was introduced for the first time in FASTEM-3 of RTTOV-8. The model was developed from measurements by the WindRad radiometer operated by Jet Propulsion Laboratory

and a model proposed by St. Germain and Poe (1998) from aircraft measurements. FASTEM-3 uses a model function of azimuth line of sight less the wind direction. FASTEM-4 and FASTEM-5 updated the azimuthal function based on a theoretical two scale model output, so no longer based on real microwave measurements from satellites. The FASTEM-4 and FASTEM-5 azimuth model function use RWD as inputs to express the azimuthal variation instead of the azimuth line of sight less the wind direction. FASTEM-3 and FASTEM-5 use harmonic cosine functions to express the variation. The Meissner and Wentz (2012) model function uses similar harmonic cosine functions for the modelling.

Our RWD model uses a second-order harmonic expansion. The approach is similar to Wentz (1992). The RWD model is a function of RWD and surface wind speed and independent from other geophysical parameters (e.g., surface temperature, boundary layer stability). This approximation is commonly used in other microwave emissivity models. It is possible that the azimuthal variation depends on any other parameters, such as significant wave height, ocean current, or boundary layer stability. But those are beyond our present study scope. The emissivity variations are modelled as follows:

$$\Delta E_i = E_{i1}\cos\phi_{\mathrm{r}} + E_{i2}\cos 2\phi_{\mathrm{r}}, \qquad \mathrm{i = v\ or\ h.} \tag{1}$$

$$E_{\mathrm{v1}} = a_{\mathrm{v1}}\left\{\exp(-\alpha_{\mathrm{v}}W^2) - 1\right\}(b_{\mathrm{v1}}W + c_{\mathrm{v1}}W^2 + d_{\mathrm{v1}}W^3), \tag{2}$$

$$E_{\mathrm{v2}} = a_{\mathrm{v2}}W, \tag{3}$$

$$E_{\mathrm{h1}} = a_{\mathrm{h1}}W, \tag{4}$$

$$E_{\mathrm{h2}} = a_{\mathrm{h2}}\left\{\exp(-\alpha_{\mathrm{h}}W^2) - 1\right\}(b_{\mathrm{h2}}W + c_{\mathrm{h2}}W^2 + d_{\mathrm{h2}}W^3), \tag{5}$$

where ΔE_i is the azimuthal variation of the microwave ocean emissivity for vertical or horizontal polarization channel. $\phi_{\mathrm{r}} = \phi_{\mathrm{w}} - \phi_{\mathrm{s}}$ is the RWD defined from wind direction ϕ_{w} and satellite azimuth angle ϕ_{s}. W is the surface wind speed in m s^{-1}. The coefficients $a_{\mathrm{v1}}, b_{\mathrm{v1}}, c_{\mathrm{v1}}, d_{\mathrm{v1}}, \alpha_{\mathrm{v}}, a_{\mathrm{v2}}, a_{\mathrm{h1}}, a_{\mathrm{h2}}, b_{\mathrm{h2}}, c_{\mathrm{h2}}, d_{\mathrm{h2}},$ and α_{h} were determined from fitting of the model to observed azimuthal variation for each frequency.

2.2 Used data and Methodology

In order to determine the coefficients of the RWD model function, truth data of microwave radiance and surface wind vector are necessary. In the literature (Wentz, 1992, Meissner and Wentz, 2002, and Meissner and Wentz, 2012), collocated data between satellite microwave measurements and buoy wind data, or microwave measurements and scatterometer wind data were used. The amount of the collocated data between different platforms is very limited and it is difficult to collect a sufficient data sample covering varied meteorological condition (e.g., from low wind speed to high wind speed) with a short period. In this study, we use simultaneous measurements of radiance and wind vector by the Advanced Earth Observing Satellite-II (ADEOS-II). The Advanced Microwave Scanning Radiometer (AMSR) and NASA scatterometer SeaWinds were aboard the satellite. The ADEOS-II data is available for seven months (April to October in 2003). Temperature and specific humidity profiles and surface temperature from ECMWF reanalysis data (ERA Interim, Dee *et al*., 2011) were used for simulation of AMSR brightness temperature in radiative transfer calculations. Ebuchi (2006) reported on the accuracy of ADEOS-II SeaWinds wind data. No systematic biases in the wind speed and direction against buoy were confirmed. Root Mean Square (RMS) differences of

the wind speed and direction were approximately 1 m s^{-1} and 20 degree in the buoy wind speed higher than 3 m s^{-1}. Moreover, SeaWinds wind data had less correlation on thermal condition of the sea surface and the sea state. SeaWinds wind data are used as the inputs of surface wind information in the radiative transfer calculations and the model function developed in our study.

The radiative transfer calculations were performed in clear sky condition with RTTOV-10, but the azimuthal function in FASTEM-5 was turned off to visualize the azimuthal variation in the difference of the observed and simulated AMSR brightness temperatures. The AMSR channels cover the microwave frequency range from 6 GHz to 89 GHz. The precise frequencies used in space based microwave imagers vary from sensor to sensor. Table 1 summarizes the frequencies and channel number, for available microwave imagers in the data assimilation. Hereafter, we use notations defined in Table 1 to specify microwave imager channels.

To separate cloud signal and surface signal in the observed AMSR brightness temperatures over oceans, cloud free scenes were selected. We used an empirical cloud screening method. We define two indexes (Sidx and Pidx) as following equation:

$$\mathrm{Sidx} = (T_{23\mathrm{V}} - T_{19\mathrm{V}}) - \mathrm{Cs} \cdot (T_{23\mathrm{V}} - T_{37\mathrm{V}}), \tag{6}$$

$$\mathrm{Pidx} = (T_{89\mathrm{H}} / T_{89\mathrm{V}}) - \mathrm{Cp} \cdot (T_{23\mathrm{V}} - T_{19\mathrm{V}}), \tag{7}$$

where $T_{19\mathrm{V}}, T_{23\mathrm{V}}, T_{37\mathrm{V}}, T_{89\mathrm{V}},$ and $T_{89\mathrm{H}}$ are observed AMSR brightness temperatures. We select AMSR data satisfying following criteria:

$$\mathrm{Smin} < \mathrm{Sidx} < \mathrm{Smax}, \tag{8}$$

$$\mathrm{Pmin} < \mathrm{Pidx} < \mathrm{Pmax}, \tag{9}$$

where $\mathrm{Cs} = 30.0/40.0, \mathrm{Cp} = 0.2/30.0, \mathrm{Smin} = 20.0, \mathrm{Smax} = 24.5, \mathrm{Smin} = 0.65$, and $\mathrm{Pmax} = 0.72$. These thresholds were empirically determined. Moreover, we require that the difference of the observed and simulated brightness temperature should be within 5.0 K to avoid cloud contamination. Sun glint affected data in AMSR data were removed in advance.

Conversion coefficients β_i from the brightness temperature to the emissivity are necessary to obtain the final coefficients used in our model.

$$\Delta T_B = \beta_i \Delta E_i. \tag{10}$$

The coefficients β_i were determined by using typical atmospheric profiles to be consistent the amplitudes of the variation between observed and simulated brightness temperature. This is possible because we assume the RWD model function is purely dependent on surface wind and there is no dependency on sea surface temperature and atmospheric properties. Because high frequency channels, e.g., 89 GHz, are sensitive to clouds in the atmosphere, the seven month ADEOS-II period was not sufficient to estimate the azimuthal variation in the all wind speed categories. Therefore, we used all-sky F17 SSMIS data instead of AMSR for the 89 GHz channels. The SSMIS has 91 GHz vertical and horizontal polarized channels. The simulated all-sky SSMIS data was obtained from ECMWF Integrated Forecasting System (IFS), using cycle 38r2 and run at a horizontal resolution T511 (with a 32 km grid) L137 (with 137 vertical levels) compared to operational resolution in June 2013 of T1279 (with a 16 km grid) L137. No azimuthal model function in the radiative transfer model (RTTOV-10) was used. We determined all the coefficients for 6, 10, 19, 37, and 89 GHz in

vertical and horizontal polarization. A linear interpolation in frequency is used to obtain intermediate frequencies (e.g., 23 GHz) needed for other microwave instruments. Thus, our RWD model function is applicable to the Advanced Microwave Scanning Radiometer for Earth Observing System (AMSR-E, Kawanishi *et al*., 2003), SSMIS and TMI that are actively used in data assimilation.

After subtraction of the mean bias in the difference of observed and simulated AMSR brightness temperature for all wind speed categories (1m s^{-1} intervals, from 0 to 18 m s^{-1}), the remaining biases are attributed to the wind directional signal in terms of RWD. Figure 1 shows the variations in terms of RWD for a surface wind speed of 12 m s^{-1}. In each panel, the vertical axis indicates the difference between observed and simulated brightness temperature after the bias subtraction. The horizontal axis is RWD defined from SeaWinds wind direction and AMSR azimuth angle. Figure 1 (a) panels are vertical polarization channels and Figure 1 (b) panels are horizontal polarization channels. Our RWD model function was fitted to the bias between the observed and simulated brightness temperature. The fitting was performed for a wind speed range from 0 to 18 m s^{-1} in 1 m s^{-1} intervals to obtain the wind speed dependency for the coefficients.

Small discrepancies with respect to our RWD model function were found close to 0 degrees in RWD in low frequency channels (06V, 06H, 10V, and 10H). They might be instrument calibration issues. Moreover, a small phase shift between measured RWD signal and fitted model function exists. The phase shift was pronounced in high wind speed condition (> 12 m s^{-1}). At present, we don't know the reasons of these discrepancies. However, the small phase shifts did not affect for the estimation of the amplitude of the variation in the wind speed range.

Figure 2 shows the coefficients obtained from the fitting for the RWD model function. The coefficients of the first harmonic term are shown in black solid circles. The second harmonic term are shown in white squares. Fitted functions of the first coefficient are drawn with solid lines and those of the second coefficients are drawn with dotted lines. The first harmonic term is dominant for vertical polarization channels and the second harmonic term is dominant for horizontal polarization channels. These results are consistent with other investigations (Meissner and Wentz, 2002, Meissner and Wentz, 2012). Large variations of the directional signal in brightness temperature are found. Moreover, wind directional signals for the high frequency channels (89V and 89H) are found, while the FASTEM-5 azimuth model function has very weak sensitivity for these channels (Figure 4). Table 2 shows the estimated coefficients for the dual polarization channels of AMSR from 6 GHz to 89 GHz. Tangent linear and adjoint models of the RWD model function were developed for use in variational data assimilations.

2.3 Comparison with other RWD model function

We compared our RWD model function performance with other azimuthal model functions. Currently, FASTEM-5 and FASTEM-3 have different azimuthal model function for the data assimilation. Figure 3 indicates calculated emissivity variation from our RWD model function for 6, 10, 19, 37 and 89 GHz at wind speeds for 0, 8, 12, 14, and 18 m s^{-1}. Figure 4 and Figure 5 are as Figure 3 but for the FASTEM-5 and FASTEM-3 azimuthal model function, respectively. Right vertical axes are scaled in Kelvin in the Figures. The mean biases in each wind speed categories were subtracted to show only the azimuthal variation. Comparing Figure 3 and Figure 4, we found that our RWD model function has larger amplitude in terms of wind speed than FASTEM-5. Our RWD model function was derived from real microwave brightness temperature measurements, while FASTEM-5 was based on a theoretical two scale model simulation results. The amplitudes of FASTEM-3 are similar to our RWD model. However, FASTEM-5 and also FASTEM-3 have sensitivity in 0 m s^{-1} wind speed range (less than 0.5 m s^{-1}). This is unphysical behaviour. We designed our RWD model function to have null sensitivity on the azimuthal variation at 0 m s^{-1} wind

speed because there is less wind direction signal in passive microwave measurements in such low wind speed situations.

Measurements on the incidence angle dependency of the azimuthal variation are very limited, so we imported them from other studies (Equation (26) in (Meissner and Wentz, 2012)) to add incidence angle dependency in our RWD model. This function is necessary to apply our RWD model function to cross-track microwave radiometers.

Over wind speed 18 m s^{-1}, ADEOS-II could not provide sufficient data for the fitting. For the high wind speed cases (> 18 m s^{-1}), our RWD model assumes that the azimuthal variation has the same amplitude as for a wind speed of 18 m s^{-1}. No extrapolation with wind speed is used. Moreover, our model does not have capability to calculate azimuthal variation on the third and fourth Stokes parameters.

3. Impact study

3.1 Experimental configuration

To examine the effect of the RWD model function in the data assimilation, we performed a data assimilation experiment in ECMWF IFS. In ECMWF IFS, microwave imager brightness temperature data are assimilated in an all-sky approach over ocean (Bauer *et al*., 2010, Geer *et al*., 2011, and Geer and Bauer, 2011). ECMWF IFS system (cycle 38r2, Bauer *et al*., 2013) uses RTTOV-10 (Saunders *et al*., 2012), as radiance observation operator in the data assimilation (Bormann *et al*., 2011). We modified the FASTEM-5 azimuthal model function with our RWD model function for the experiment. The Control run does not use the azimuthal function in FASTEM-5 for the microwave imagers. As for microwave sounders (e.g., AMSU-A, MHS), the azimuthal model function in FASTEM-5 is used in the Control run. These are consistent with the operational ECMWF IFS configuration. Our RWD model function is used for microwave imager and sounder instruments in the Test run. Because the surface sensitive channels (e.g., AMSU-A, channel 1, 2, 3, and 4, MHS channel 1 and 2) are not actively assimilated in the ECMWF system, the change of the emissivity model for the microwave sounders should be minor and major impact would be seen for the microwave imagers.

The input RWD for the model is the difference between first guess wind direction and the satellite azimuth angle at the observation locations. SSMIS and TMI do not have azimuth angles available in the real time data set, so the angles were numerically calculated in house using the Kumabe and Egawa (2011) method from the satellite sensor position and scan geometry.

Observations used in the experiments are identical between the Test run and the Control run. Quality control, pre-screening and the forecast model are also identical between the two runs. The only difference is the use of the RWD model function in the radiative transfer calculation. The experiment was executed at T511 L137 resolution with cycle 38r2 configuration. This was the operational cycle at ECMWF in June 2013, but in our experiments it was run at approximately half the operational resolution. The experiment period was from 20 June to 3 October 2011. The forecasts from 00 UTC initial time were produced every day during the period. Because three microwave imagers (AMSR-E, TMI and F17 SSMIS) were available in the experiment period, the large amount of radiance data would provide a strong test for the use of the RWD model function. The microwave imager channels 19V, 19H, 23V, 23H (for AMSR-E only), 37V, and 89V were actively assimilated in the experiment. AMSR-E 89V and 89H channels were not available due to instrument issues during the period. In the

ECMWF all-sky radiance assimilation scheme, horizontal polarization channels at 37 GHz and 89 GHz from microwave imagers are not assimilated.

3.2 FG departure comparison

The first guess (FG) departure is examined to investigate the impact of the RWD model function in the radiative transfer calculations. Figure 6 (a) panels show bias (black dots for the Test and open circle for the Control) and standard deviation (solid bars for Test and dotted for Control) for AMSR-E 19V FG departure at wind speed (4, 8, 10, 12, 14, and 16 m s^{-1}) categories. We used FG departure after variational bias corrections (VarBC, Dee 2004) for these comparisons. In low wind speed condition (e.g., 4 m s^{-1}), the differences between the Test run and the Control run were small because the azimuthal variation itself was small. In high wind speed condition (> 10 m s^{-1}), clear azimuthal variations in terms of RWD were found in the Control run. This means NWP FG wind field has sufficiently high accuracy in speed and direction to represent the azimuthal variation. The azimuthal variations in the biases were reduced in the Test run. Figure 6 (b) panels show the same results but for 19H. In high wind conditions (e.g., 16 m s^{-1}), the biases from the azimuthal variation reached about 2 K in the Control run in both polarizations. However, in the Test run, the RWD model function was able to represent the variation for both polarizations from the low to high wind speed conditions and reduced the biases. Although the results in high wind conditions (Figure 6 (b) 14 m s^{-1}, 16 m s^{-1}) show small remaining biases, generally most of the biases were reduced in the Test run. Figure 6 (c) panels indicate comparisons among different frequency (19V, 19H, 23V, 23H, 37V, and 89V) at 12 m s^{-1} wind speed condition. These microwave imager channels are actively assimilated in the ECMWF IFS. At 89V, the results for SSMIS were plotted instead of AMSR-E. For the frequency range from 19 GHz to 91 GHz, the RWD model function reduced the biases and worked properly for AMSR-E, SSMIS, and TMI.

Figure 7 (a) and (b) show geographical distributions of mean FG departure of assimilated F17 SSMIS 19V in the Control run. Moreover, (c) and (d) show standard deviation of the FG departure. Figure 7 (a) and (c) are ascending data and (b) and (d) are descending data. In the Intertropical Convergence Zone (ITCZ) and South Pacific Convergence Zone (SPCZ), large positive biases (2 - 5 K) in FG departure were found for both ascending and descending orbit data (Figure 7 (a), (b)). Moreover, in the ITCZ and SPCZ, the standard deviations were larger than other areas. The reason for the positive biases and the large standard deviation relates both to the accuracy of the radiative transfer model and the forecast model under cloud and precipitation conditions. They are similar in ascending and descending orbits. Because larger observation errors are assigned for these data in ECMWF all-sky radiance assimilation system (Geer and Bauer 2011), these biases are not as important as they look. However, the FG departure bias in the Arabian Sea was orbit dependent. The sign of the bias was opposite between the ascending orbit (negative bias approximately 1.5 K) and descending orbit (positive bias approximately 1.0 K) while the standard deviations in the area were relatively small (less than 2 K) compared with other areas. The orbit dependent biases are large and might have a negative impact in the Control run.

Figure 8 shows the difference of mean FG departure between the Test and Control run for F17 SSMIS 19V (a) ascending and (b) descending data. The impacts of the RWD model function varied between regions and orbital direction in the SSMIS FG departures. Generally, the orbit dependent biases of the microwave imagers in the Control run were reduced in the Test run. The bias reduction in the Arabian Sea was remarkable. The bias reductions in the ascending and descending data in the Arabian Sea were approximately 0.6 K and 0.7K, respectively. Moreover, the biases in Northeast (NE) Pacific, Southeast (SE) Pacific, and SE Atlantic oceans were also reduced. The change in the southern hemisphere (latitude 60 degree south, along storm track) were opposite between the ascending (negative) and the descending orbit (positive) because westerly winds were dominant in

this area. Figure 8 (c) and (d) are Metop-A AMSU-A channel 5 ascending and descending data, respectively. Figure 8 (e) and (f) are Metop-A MHS channel 5. These channels are the lowest tropospheric channel actively assimilated of the microwave sounding instruments. The change of the emissivity affects the simulated brightness temperature of the microwave sounding channels. Figure 8 (c), (d), (e), and (f) does not show any surface related geographical pattern both in ascending and descending data. Furthermore, although the window channels of the microwave sounding instruments are used in the quality-controlling of the lower tropospheric channels in the ECMWF system, the differences of the assimilated data counts between the Test and Control run were very small (e.g., approximately 0.05 % difference for AMSU-A channel 5 and 0.01 % difference for MHS channel). The impacts of the RWD model function were minor for the microwave sounding data. However, major impacts were found for the microwave imager data.

To confirm the relationship of the changes in the FG departure biases of the microwave imager channels and the surface wind field, monthly mean 1000 hPa wind field for August 2011 from the analysis in the Test is shown in Figure 9. In the experiment period (boreal summer), the strong south-westerly winds (Somali jet) in the Arabian Sea is clearly seen. The Somali jet is a high wind speed meteorological phenomenon with mean winds of more than 12 m s^{-1} from June to September every year. Moreover, this area is generally cloud free in the boreal summer. The microwave imagers observe the surface directly without any cloud and rain contamination. The negatively biased area shown in Figure 7 (a) has a good agreement with the high wind area (> 10 m s^{-1}) in Figure 9. Moreover, other large difference areas in FG departure seen in Figure 8 (a) and (b) correspond to areas with high wind speed and low wind direction variability.

Figure 10 shows standard deviations of FG departures of microwave imagers (AMSR-E, TMI, and SSMIS) for three regions (Northern Hemisphere, Tropics and Southern Hemisphere). Standard deviations have been normalized by the value of the Control run and shown in percentage. Generally, the standard deviations of FG departures were reduced in the Test run globally. The reductions of FG departure of vertical polarization channels in the southern hemisphere were significant. One reason of the larger impact is that high wind speed areas occur more often in the southern hemisphere than in mid- and low- latitudes during the experiment period.

Figure 11 shows the satellite azimuth angle (a), (b) and the relative wind direction (c), (d) for AMSR-E for the Arabian Sea. Although this is a single day in the experiment period, the pattern of the satellite azimuth angle and the RWD are similar during the period because conical scanning microwave imagers on polar orbiting satellites observe the area with this fixed geometry every orbit. For the Arabian Sea, the value of RWD in ascending orbit (Figure 11 (c)) is from 180 to 240 (downwind direction) degrees and that of in descending orbit (Figure 11 (d)) is around 0 or 360 degree (upwind direction). The azimuthal variation in term of RWD has a minimum in the downwind direction (19V) and a maximum in the upwind direction as shown in Figure 1 (a). The orbit dependent biases shown in Figure 7 were caused with non-modelling of RWD variation in the Control run. In the Test run, the biases caused by the azimuthal variation were reduced with the RWD model function in the radiative transfer calculations.

3.3 Impacts on atmospheric analysis and forecast

The microwave imager channels (19V, 19H, 23V, 23H, 37V, and 89V) have strong sensitivity not only to surface wind but also to atmospheric humidity and cloud in the lower troposphere. The humidity information obtained from the microwave measurements plays an important role in the humidity analysis and forecast. As most of the water vapour amounts are concentrated in the lower troposphere, we investigated mean difference of the RMS of analysis increments on the 1000 hPa specific humidity (Figure 12). The largest reduction of the RMS of the analysis increment was found

for the Arabian Sea (approximately, 0.3 g kg^{-1}). In the high latitude areas in the southern hemisphere (along the storm track), the impact was small compared with other high wind speed areas. Although there are high wind areas in the southern hemisphere, many microwave imager observations are not used because of large positive biases caused by a lack of cloud liquid water in cold sectors (Geer and Bauer, 2011) in the ECMWF forecast fields.

The use of the RWD model function brought improvements in the forecast. Figure 13 shows normalized differences of RMS error of relative humidity (RH) and temperature (T) forecasts. The forecasts were verified against the experiment's own analysis. Blue colours indicate a reduction in the forecast error arising from the use of the RWD model function in the radiative transfer calculations. In the southern hemisphere lower troposphere, significant error reductions in relative humidity and temperature were found for short-range forecasts. The improvements of the RMS error at 12 hour forecast indicate reductions of analysis increments of relative humidity and temperature in the data assimilation.

Figure 14 shows the normalized RMS error difference of relative humidity as a function of forecast time for three pressure levels (500, 850, and 1000 hPa). Significant improvements were found in the southern hemisphere and the tropics in the short-range forecasts. The improvements in the southern hemisphere lower troposphere were retained until day 3 of the forecast.

Figure 15 is as Figure 14 but for temperature forecasts in the lower troposphere. Significant improvements of the temperature were found in the southern hemisphere and the tropics. However, the improvements were limited in day 1 of the forecast. The results indicate the improvements in the short-range forecast could have been driven by the reductions of the humidity analysis increment in the data assimilation.

4. Summary and Conclusion

In this study, we focussed on the wind directional signals in the oceanic microwave radiance data. The azimuthal variation is a well-known phenomenon and many applications in remote sensing utilize it in geophysical product retrievals. However, the wind direction signals have not been actively taken into account in the radiative transfer calculation in data assimilation. ECMWF IFS FG fields do have sufficient accuracy to detect the azimuthal variation in the FG departure (shown in Figure 6 Control run results).

To utilize the wind direction signal in the data assimilation, a new RWD model function was developed for the emissivity model. The development was based on simultaneous measurements of microwave radiance and surface wind vector from ADEOS-II AMSR and SeaWinds. Cloud-free conditions were selected to separate the surface signals and the atmospheric signals in the observations. As for cloud sensitive channels (89V and 89H), all-sky SSMIS data were used. The developed RWD model function was incorporated into the microwave ocean emissivity model (FASTEM-5) in RTTOV-10 for the impact study.

Input RWD was calculated from the surface wind vector in the FG field and the satellite azimuth angle. Because the satellite azimuth angles of SSMIS and TMI were not available in the real time data in ECMWF IFS, the angles were calculated from the satellite position and the scan geometry in house. As the azimuth angle information is one of the basic satellite parameters for the radiative transfer calculation and other remote sensing applications, the information should be included in the operational data set by space agencies for future microwave imagers.

The RWD model function performances were different from those of FASTEM-5 and FASTEM-3. The performance of our RWD model function shown in Figure 3 brought reduction of the FG departure biases (shown in Figure 6) in the experiment. It is difficult to expect that the small amplitude of FASTEM-5 (Figure 4) and the unphysical wind direction sensitivity at low wind speed of FASTEM-3 (Figure 5) can provide better performance than our RWD model function. Because our RWD model function is based on real satellite measurements, we believe our model is more realistic than other models under low wind speed conditions and for high frequency channels. The model function can be used for other microwave imagers (e.g., AMSR-E, SSMIS and TMI) and sounders (e.g., AMSU-A, MHS). The RWD model function reduced the FG departure biases in the Test run, especially in high wind speed and low wind direction variability areas (i.e., Arabian Sea, NE Pacific, SE Pacific, SE Atlantic oceans) for the microwave imagers. The impacts for the microwave sounding data were minor.

The orbit dependent biases of the microwave imagers in the Control run were caused by non-modelling of the azimuthal variation in the emissivity calculations. However, the Test run had lower biases. This is confirmed from the reduction of the analysis increment of the specific humidity at 1000 hPa. The changes in high wind speed areas lead to a significant improvement in RMS errors of the relative humidity and temperature fields in lower troposphere for short-range forecasts.

The changes in FG departure using our new RWD model function were consistent with wind field and satellite azimuth angle relationship. Currently, the use of microwave imager radiance data in the southern hemisphere is limited due to cold sector biases (Geer and Bauer 2011) in the ECMWF system. To enhance the use of the microwave imager data in the high latitude areas in future, the azimuthal variation should be treated with an accurate RWD model function in the radiative transfer model. The experiment results clearly showed the importance of the modelling of the azimuthal variation in the microwave radiance assimilation. The RWD model function should be in the radiative transfer model both for present microwave imagers and for upcoming new sensors; e.g., Global Change Observation Mission - Water1 (GCOM-W1) AMSR2 and the Global Precipitation Measurement Microwave Imager (GMI).

Appendix

There are varying definitions used for the azimuthal wind and satellite angles. This appendix clarifies the situation; in particular the difference between FASTEM-5 and FASTEM-3, and it defines the angles used in the new relative wind direction (RWD) model function.

The satellite azimuth angle ϕ_s is defined using satellite location and observation location as Figure 16 (a). The satellite azimuth angle is used as input for the radiative transfer calculation (RTTOV). In RTTOV, microwave ocean emissivity module (FASTEM) calculates the emissivity for each channel (vertical, horizontal polarization, and the third and the fourth Stokes parameters). The input satellite azimuth angle ϕ_s is passed to the FASTEM. Azimuthal angle information used in FASTEM is calculated from the satellite azimuth angle ϕ_s and surface wind direction (10 m wind direction from NWP FG field). The definition of the azimuthal angle information is different between FASTEM-5 and FASTEM-3. FASTEM-4 azimuthal model function is same with FASTEM-5 azimuthal function.

As shown in Figure 16 (a), the satellite azimuth angle ϕ_s and satellite azimuth view (looking) angle ϕ_v are related as follows:

$$\phi_v = \phi_s + 180. \quad (11)$$

The angles are measured clockwise from North and described from 0 to 360 degree range as shown in Figure 16 (a).

In FASTEM, 10 m wind direction ϕ_w is defined as a direction towards which the wind is blowing. In meteorological convention, wind direction ϕ_m is defined as a direction from which the wind is blowing (Figure 16 (b)). The FASTEM wind direction ϕ_w and the meteorological wind direction ϕ_m are related as follows:

$$\phi_m = \phi_w + 180. \quad (12)$$

The wind directions are measured clockwise from North and described from 0 to 360 degree range.

FASTEM-5 uses RWD as input azimuthal angle information. RWD ϕ_r is defined as wind direction relative to the satellite azimuth angle. RWD is defined as follows:

$$\phi_r = \phi_w - \phi_s, \quad (13)$$

where ϕ_w is FASTEM wind direction and ϕ_s is the satellite azimuth angle. Our RWD model function uses ϕ_r as input azimuthal angle information. The range of ϕ_w and ϕ_s are from 0 to 360 degree. RWD ϕ_r is described in 0 to 360 degree range. Using Eq. (11) and Eq. (12), Eq. (13) can be written as follows:

$$\phi_r = \phi_m - \phi_v. \quad (14)$$

Eq. (14) indicates that RWD can be calculated from the meteorological wind direction and the satellite azimuth view angle. Figure 16 (c) illustrates the definition of RWD ϕ_r in a westerly wind case using the FASTEM wind direction ϕ_w and the satellite azimuth angle ϕ_s.

On the other hand, FASTEM-3 uses azimuth line of sight less the wind direction (Saunders *et. al.*, 2006) as the azimuthal angle information. The angle $\phi_{r(FASTEM-3)}$ is defined as follows:

$$\phi_{r(FASTEM-3)} = \phi_s - \phi_w. \quad (15)$$

However, the coding in RTTOV-10, actual input is defined as follows:

$$\phi_{r(FASTEM-3)} = 180 - (\phi_w - \phi_s). \quad (16)$$

By using Eq. (11), Eq. (16) can be written as follows:

$$\phi_{r(FASTEM-3)} = \phi_v - \phi_w. \quad (17)$$

Eq. (17) implies that FASTEM-3 azimuthal model function in RTTOV uses satellite azimuth view angle ϕ_v. This is an inconsistency in the present RTTOV coding and FASTEM-3 definition. In this study, we use correct input for azimuthal variation calculation for FASTEM-3 (results shown in Figure 5).

Acknowledgement

This study was carried out under through a collaboration between ECMWF and the Japan Meteorological Agency (JMA). The authors acknowledge Alan Geer of ECMWF for his insightful comments and discussions. The authors would like to thank Akira Shibata of the Meteorological Satellite Center, JMA for providing the collocated ADEOS-II AMSR and SeaWinds data and valuable comments on this research topic. Takumu Egawa of JMA kindly provided the technical information on the satellite azimuth angle calculations. This work was funded by a Fellowship Program by the Ministry of Education, Culture, Sports, Science and Technology of the Japanese Government.

References

Bauer P, Geer AJ, Lopez P, Salmond D. 2010. Direct 4D-Var assimilation of all-sky radiances. Part I: Implementation. *Q.J.R. Meteorol. Soc.*, **136**: 1868–1885. DOI: 10.1002/qj.659.

Bauer, P., Beljaars A, Ahlgrimm M, Bechtold P, Bidlot JR, Bonavita M, Bozzo A, Forbes R, Hólm E, Leutbecher M, Lopez P, Magnusson L, Prates F, Rodwell M, Sandu I, Untch A, Vitart F. 2013. `*Model Cycle 38r2: Components and Performance*,` ECMWF Tech. Memo. 704. ECMWF: Reading, UK. Available at http://www.ecmwf.int.

Bormann N, Geer A, Wilhelmsson T. 2011.`*Operational implementation of RTTOV-10 in the IFS*,` ECMWF Tech. Memo. 650. ECMWF: Reading, UK. Available at http://www.ecmwf.int.

Bormann N, Geer A, English S. 2012. `*Evaluation of the microwave ocean surface emissivity model FASTEM-5 in the IFS*,` ECMWF Tech. Memo. 667. ECMWF: Reading, UK. Available at http://www.ecmwf.int.

Deblonde G, English SJ. 2001. `Evaluation of the FASTEM2 Fast Microwave Oceanic Surface Emissivity Model`. *In Tech. Proceedings of International TOVS Working Group-XI, Budapest, 20 Sep - 26 Sep 2000*.

Dee D. 2004.`Variational bias correction of radiance data in the ECMWF system,` In *Proceedings of workshop on assimilation of high spectral resolution sounders in NWP*, 28 Jun - 1 Jul 2004. ECMWF: Reading, UK. http://www.ecmwf.int

Dee DP, Uppala SM, Simmons AJ, Berrisford P, Poli P, Kobayashi S, Andrae U, Balmaseda MA, Balsamo G, Bauer P, Bechtold P, Beljaars ACM, van de Berg L, Bidlot J, Bormann N, Delsol C, Dragani R, Fuentes M, Geer AJ, Haimberger L, Healy SB, Hersbach H, Hólm EV, Isaksen L, Kållberg P, Köhler M, Matricardi M, McNally AP, Monge-Sanz BM, Morcrette J-J, Park B-K, Peubey C, de Rosnay P, Tavolato C, Thépaut J-N, Vitart F. 2011. The ERA-Interim reanalysis: configuration and performance of the data assimilation system. *Q.J.R. Meteorol. Soc.*, **137**: 553–597. DOI: 10.1002/qj.828.

Dzura MS, Etkin VS, Khrupin AS, Pospelov MN, Raev MD, `Radiometers-polarimeters: Principles of design and applications for sea surface microwave emission polarimetry`. In *Proceedings of the 1992 IEEE International Geoscience and Remote Sensing Society (IGARSS), Houston, TX 26 - 29 May 1992*. DOI: 10.1109/IGARSS.1992.578475.

Ebuchi N. 2006. Evaluation of Marine Surface Winds Observed by SeaWinds and AMSR on ADEOS-II. *Journal of Oceanography*, **62**: 293 - 301.DOI: 10.1007/s10872-006-0054-6.

English SJ, Hewison TJ. 1998. `A fast generic millimetre-wave emissivity model`. In *Proceedings of SPIE* 3503, 288-300.

Etkin VS, Raev MD, Bulatov MG, Militsky YA, Smirnov AV, Raizer VY, Trokhimovsky YA, Irisov VG, Kuzmin AV, Litovchenko KT, Bespalova EA, Skvortsov EI, Pospelov MN, Smirnov AI. 1991. `*Radiohydrophysical aerospace research of ocean*,` Academy of Science, Space Research Institute, Moscow, Russia, Tech. Rep. IIp-1749.

Geer, AJ, Bauer P, Lopez P. 2010. Direct 4D-Var assimilation of all-sky radiances. Part II: Assessment. *Q.J.R. Meteorol. Soc.*, **136**: 1886–1905. DOI: 10.1002/qj.681.

Geer, AJ, Bauer P. 2011. Observation errors in all-sky data assimilation. *Q.J.R. Meteorol. Soc.*, **137**: 2024–2037. DOI: 10.1002/qj.830.

Kawanishi T, Sezai T, Ito Y, Imaoka K, Takeshima T, Ishido Y, Shibata A, Miura M, Inahata H, Spencer RW. 2003. The Advanced Microwave Scanning Radiometer for the Earth Observing System (AMSR-E), NASDA's Contribution to the EOS for Global Energy and Water Cycle Studies. *IEEE Trans. Geosci. Remote Sens.*, **14**, 184-194. DOI: 10.1109/TGRS.2002.808331

Kumabe R, Egawa T. 2011. `*Development of a Procedure to Make Better Use of SSM/I Data Including Navigation Errors*,` Meteorological Satellite Center Technical Note, No. **55**, Japan Meteorological Agency.

Liou KN. 2002. *An Introduction to Atmospheric Radiation*. 2nd ed. Academic Press, 583pp.

Liu Q, Weng F. 2003. Retrieval of sea surface wind vector from simulated satellite microwave polarimetric measurements, *Radio Sci.*, **38** (4), 8078, DOI:10.1029/2002RS002729.

Liu Q, Weng F, English S. 2011. An Improved Fast Microwave Water Emissivity Model. *IEEE Trans. Geosci. Remote Sens.*, **49**, 1238-1250. DOI:10.1109/TGRS.2010.2064779.

Meissner T, Wentz F. 2002. An Updated Analysis of the Ocean Surface Wind Direction Signal in Passive Microwave Brightness Temperatures. *IEEE Trans. Geosci. Remote Sens.*, **40**, 1230-1240.DOI: 10.1109/TGRS.2002.800231.

Meissner T, Wentz FJ. 2012. The Emissivity of the Ocean Surface Between 6 and 90 GHz Over a Large Range of Wind Speeds and Earth Incidence Angles. *IEEE Trans. Geosci. Remote Sens*., **50**, 3004-3026. DOI: 10.1109/TGRS.2011.2179662

Monahan EC, O'Muircheartaigh IG, 1986. Whitecaps and the passive remote sensing of the ocean surface. *Int. J. Remote Sensing*, **7**, 627-642.

Saunders R, Matricardi M, Brunel P. 1999. An improved fast radiative transfer model for assimilation of satellite radiance observations. *Q.J.R. Meteorol. Soc*., **125**: 1407–1425. DOI: 10.1002/qj.1999.49712555615.

Saunders R, Andersson E, Brunel P, Chevallier F, Deblonde G, English S, Matricardi M, Rayer P, Sherlock V. 2002. `*RTTOV-7 - Science and validation report*,` v1.3, 1-51, EUMETSAT NWP-SAF.

Saunders R, Brunel P, English S, Bauer P, O'Keeffe U, Francis P, Rayer P. 2006. `*RTTOV-8 - Science and validation report,*` NWPSAF-MO-TV-007, v1.6, 1-46, EUMETSAT NWP-SAF.

Saunders R, Hocking J, Rayer P, Matricardi M, Geer A, Bormann N, Brunel P, Karbou F, Aires F. 2012. `*RTTOV-10 Science and validation report,*` NWPSAF-MO-TV-023, v1.11, 1-31, EUMETSAT NWP-SAF.

Saunders R, Hocking J, Rundle D., Rayer P, Matricardi M, Geer A, Lupu C, Brunel P, Vidot J. 2013. `*RTTOV-11 Science and validation report,*` NWPSAF-MO-TV-032, v1.11, 1-31, EUMETSAT NWP-SAF.

St. Germain K, Poe G. 1998. `*Polarimetric emission model of the sea at microwave frequencies, Part II: Comparison with measurements,*` Washington, D.C., Naval Research Laboratory Report.

Tang C. 1974. The effect of droplets in the air-sea transition zone on the sea brightness temperature. *J. Phys. Oceanography*, **4**, 579-593.

Tsang L. 1991. Polarimetric Passive Microwave Remote Sensing of Random Discrete Scatterers and Rough Surfaces. *Journal of Electromagnetic Waves and Applications*. **5**, 41 - 57.

Weng F, Han Y, van Delst P, Liu Q, Yan B. 2005. `JCSDA community radiative transfer model (CRTM)`. In *Tech. Proceedings of International TOVS Working Group- XIV, Beijing, 25 - 31 May 2005*.

Wentz FJ. 1992. Measurement of Oceanic Wind Vector Using Satellite Microwave Radiometers. *IEEE Trans. Geosci. Remote Sens.*, **30**, 960-972.

Wentz FJ. 1997. A well-calibrated ocean algorithm for special sensor microwave / imager. *Journal of Geophysical Research*, **102**, 8703-8718.

Yueh SH, Kwok R, Li FK, Nghiem SV, Wilson WJ. 1994. Polarimetric passive remote sensing of ocean wind vectors. *Radio Science*, **29**, 799-814.

Yueh SH, Wilson WJ, Li FK, Nghiem SV, Ricketts WB. 1995. Polarimetric Measurements of Sea Surface Brightness Temperatures Using an Aircraft K-Band Radiometer. *IEEE Trans. Geosci. Remote Sens.*, **33**, 85-92.

Yueh SH. 1997. Modeling of Wind Direction Signals in Polarimetric Sea Surface Brightness Temperatures. *IEEE Tans. Geosci. Remote Sens.*, **35**, 1400-1418.

Yueh, SH, Wilson WJ, Li FK, Nghiem SV, Ricketts WB. 1997. Polarimetric Brightness Temperatures of Sea Surfaces Measured with Aircraft K- and Ka- Band radiometers. *IEEE Trans. Geosci. Remote Sens.*, **35**, 1177-1187.

Yueh SH, Wilson WJ, Dinardo SJ, Li FK. 1999. Polarimetric Microwave Brightness Signatures of Ocean Wind Directions. *IEEE Tans. Geosci. Remote Sens.*, **37**, 949-959.

List of Tables

Table 1. Microwave imager channel frequency

Band	Notation	Polarization	Sensor (channel number and frequency [GHz])					
			AMSR-E		TMI		SSMIS	
			Ch	Frequency [GHz]	Ch	Frequency [GHz]	Ch	Frequency [GHz]
C	06V	V	1	6.925				
	06H	H	2	6.925				
X	10V	V	3	10.65	1	10.65		
	10H	H	4	10.65	2	10.65		
Ku	19V	V	5	18.7	3	19.35	13	19.35
	19H	H	6	18.7	4	19.35	12	19.35
K	23V	V	7	23.8	5	21.3	14	22.235
	23H	H	8	23.8				
Ka	37V	V	9	36.5	6	37	16	37
	37H	H	10	36.5	7	37	15	37
W	89V	V	11	89.0A	8	85.5	17	91.655
	89H	H	12	89.0A	9	85.5	18	91.655
		V	13	89.0B				
		H	14	89.0B				

Table 2. Estimated coefficients for the RWD model function

Channel	a_{v1}	b_{v1}	c_{v1}	d_{v1}	α_v	a_{v2}	β_v
06V	4.401E-02	-1.636E+01	1.478E+00	-4.800E-02	3.202E-06	-6.002E-05	279.72
10V	4.379E-02	-1.633E+01	1.453E+00	-4.176E-02	5.561E-06	-4.644E-05	279.72
19V	5.009E-02	-1.638E+01	1.520E+00	-3.994E-02	1.330E-05	1.113E-05	246.15
37V	5.553E-02	-1.638E+01	1.602E+00	-4.246E-02	1.903E-05	7.524E-06	222.22
89V	-9.131E-05	1.251E+00	6.769E-01	-2.913E-02	1.092E+00	-1.806E-04	126.50
Channel	a_{h1}	a_{h2}	b_{h2}	c_{h2}	d_{h2}	α_h	β_h
06H	-1.234E-07	-8.179E-03	-1.040E+01	4.477E-01	0.000E+00	3.390E-05	280.00
10H	-1.938E-05	-8.007E-03	-1.039E+01	4.610E-01	0.000E+00	4.419E-05	280.00
19H	1.362E-04	-1.013E-03	-9.235E+00	3.844E-01	0.000E+00	2.891E-04	240.00
37H	1.910E-04	-2.224E-04	-9.232E+00	3.982E-01	0.000E+00	1.673E-03	218.18
89H	3.554E-04	5.226E-04	9.816E-01	-7.783E-03	0.000E+00	2.437E+01	120.00

List of Figures

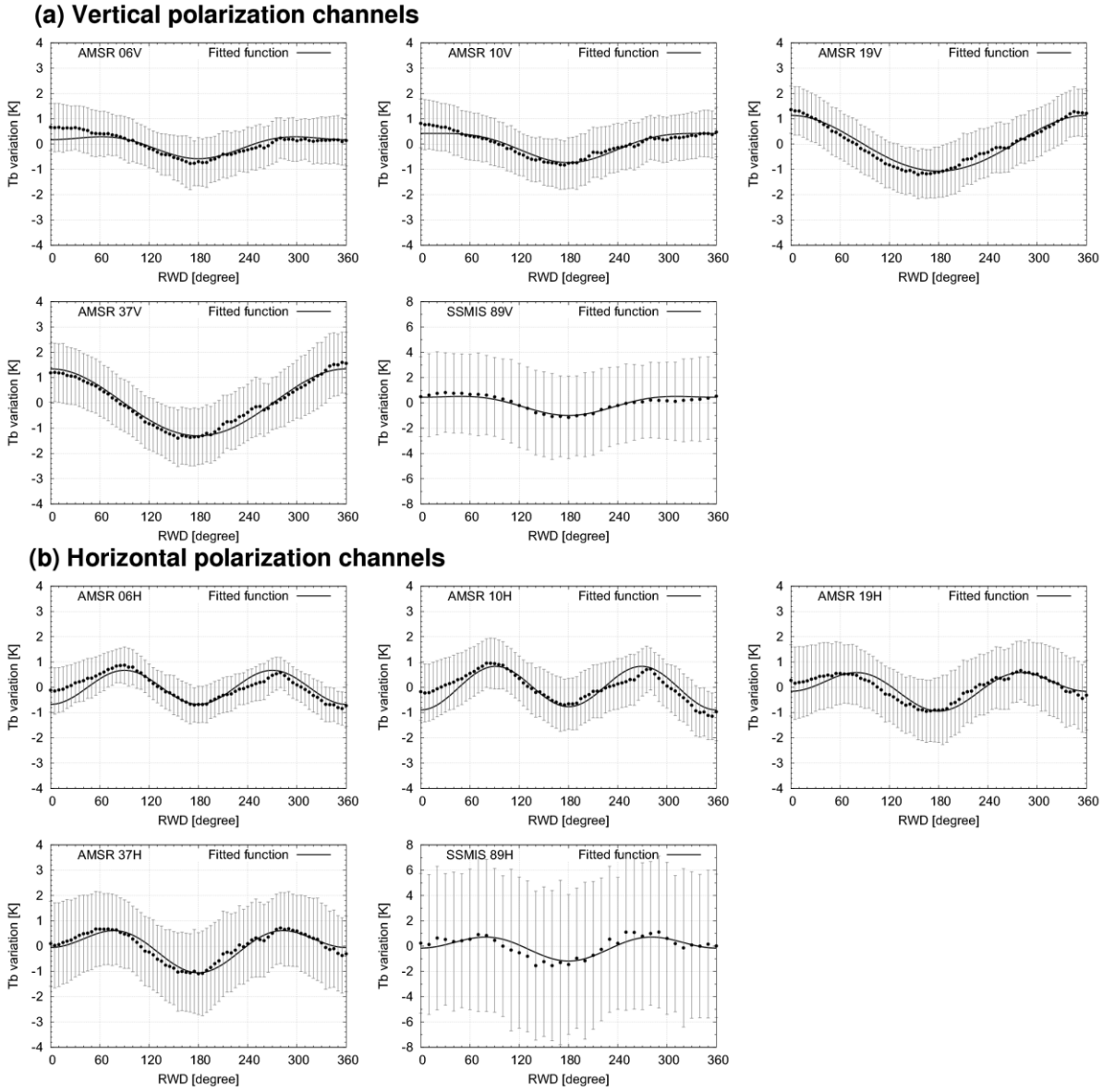

Figure 1. Oceanic microwave brightness temperature variation in terms of RWD for surface wind speed 12 m/s. (a) panels are vertical polarization channels and (b) panels are for horizontal polarization channels. AMSR brightness temperature and SeaWinds wind vector were used for 6, 10, 19, and 37 GHz. F17 SSMIS brightness temperature and surface wind vector from ECMWF IFS were used (see text section 2.2) for 89 GHz. The biases (black filled circles) and standard deviation (error bars) were plotted and fitted model functions were drawn with a black solid line.

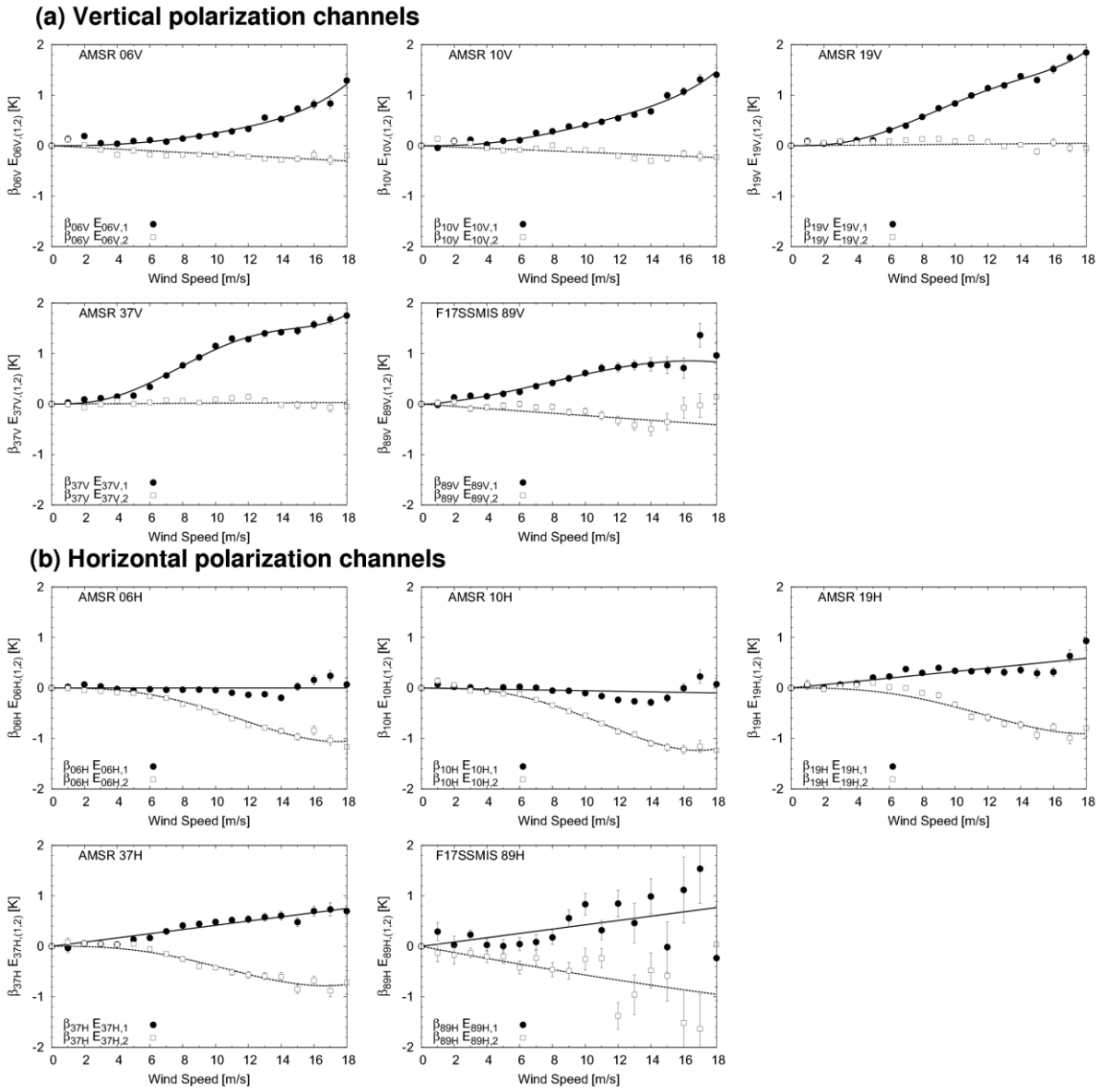

Figure 2. The amplitude of the harmonic cosine functions from the azimuthal variation. Black filled circles are the first harmonic term E_{i1} and white squares are the second harmonic term E_{i2} in Eq. (1). (a): Fitted functions in terms of wind speed for vertical channels with solid curves (Eq. (2)) and dotted curves (Eq. (3)). (b): same with (a) but for horizontal channels with solid curves (Eq. (4)) and dotted curves (Eq. (5)). 06V, 06H, 10V, 10H, 19V,19H, 37V, 37H are AMSR results and 89V and 89H are F17 SSMIS results.

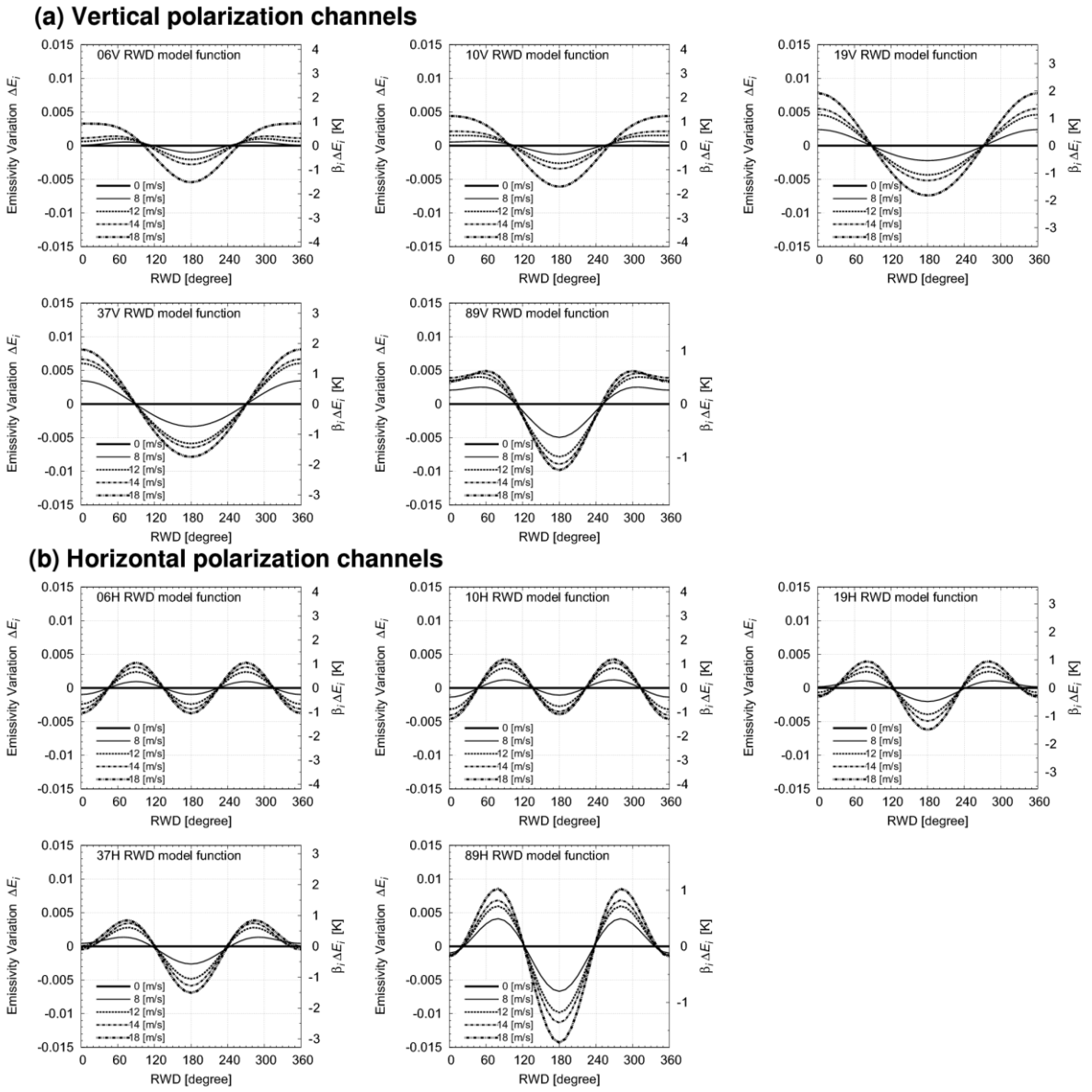

Figure 3. The azimuthal variation of the calculated emissivity with the developed RWD model function for 6 to 89 GHz. (a): vertical polarization channels at 0, 8, 12, 14, 18 m/s surface wind speed cases. (b): same with (a) but for horizontal polarization channels. Right vertical axes are scaled in Kelvin by multiplying conversion coefficient β_i.

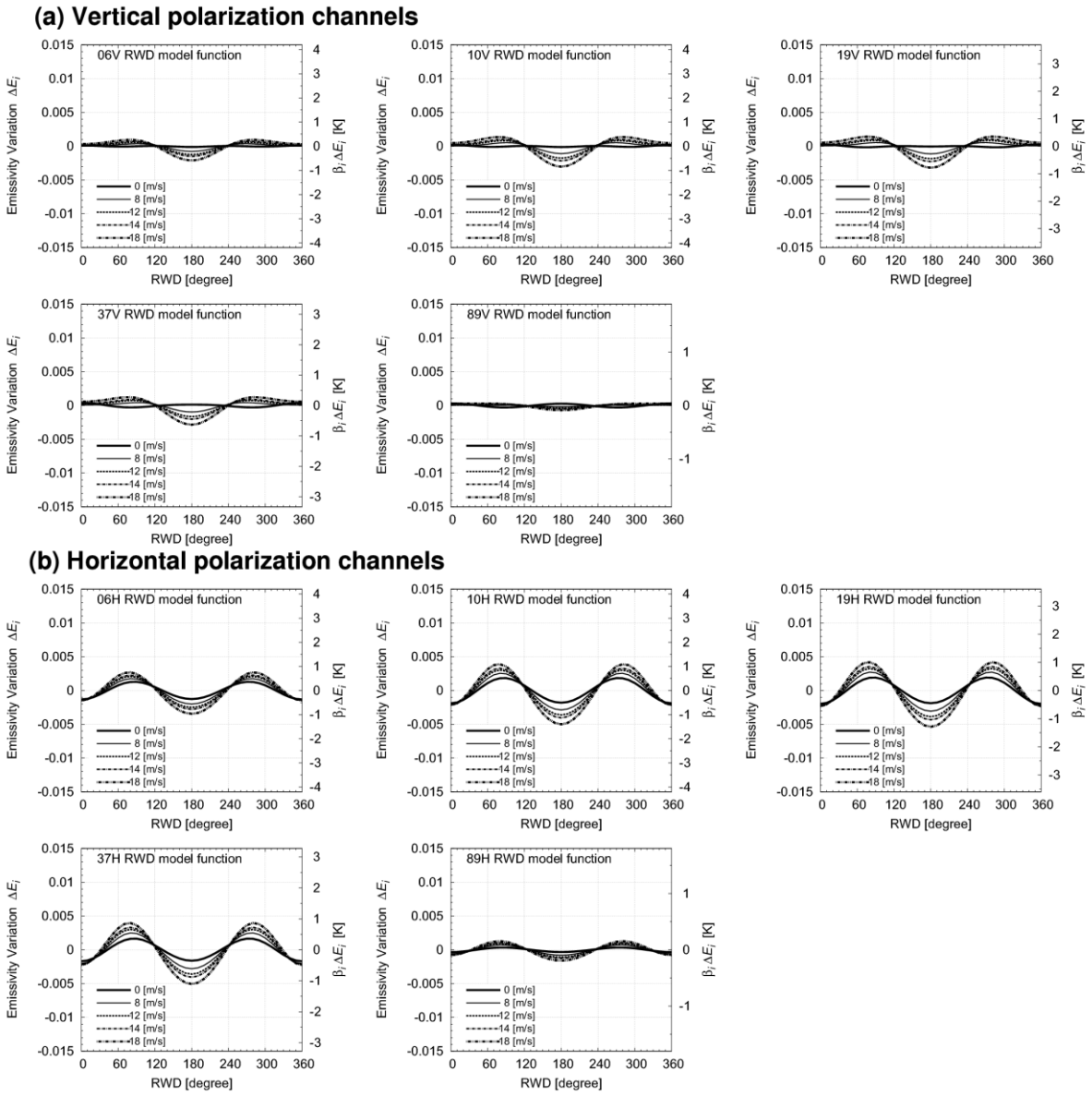

Figure 4. Same with Figure 3 but for FASTEM-5 azimuthal model function.

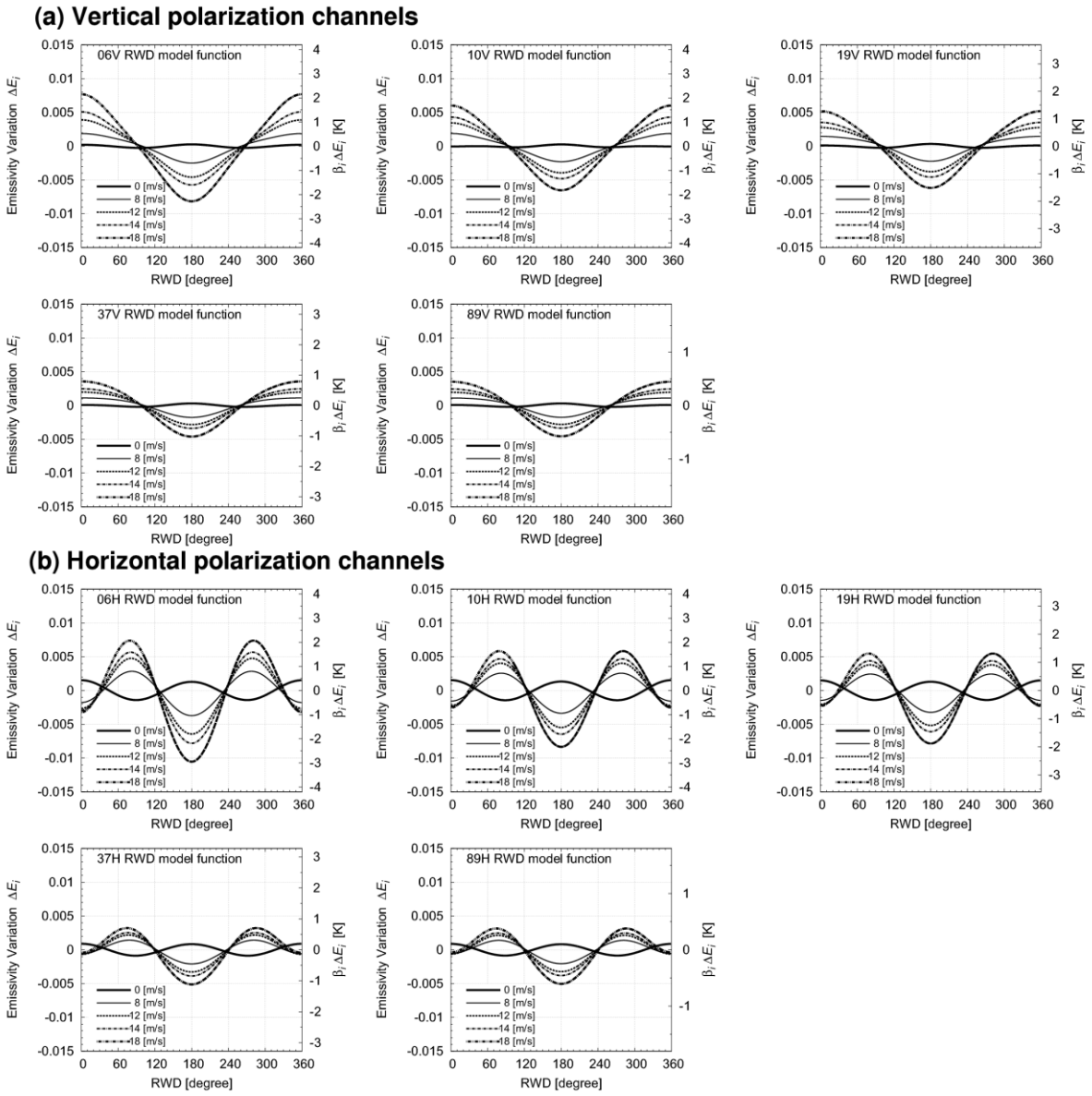

Figure 5. Same with Figure 3 but for FASTEM-3 azimuthal model function.

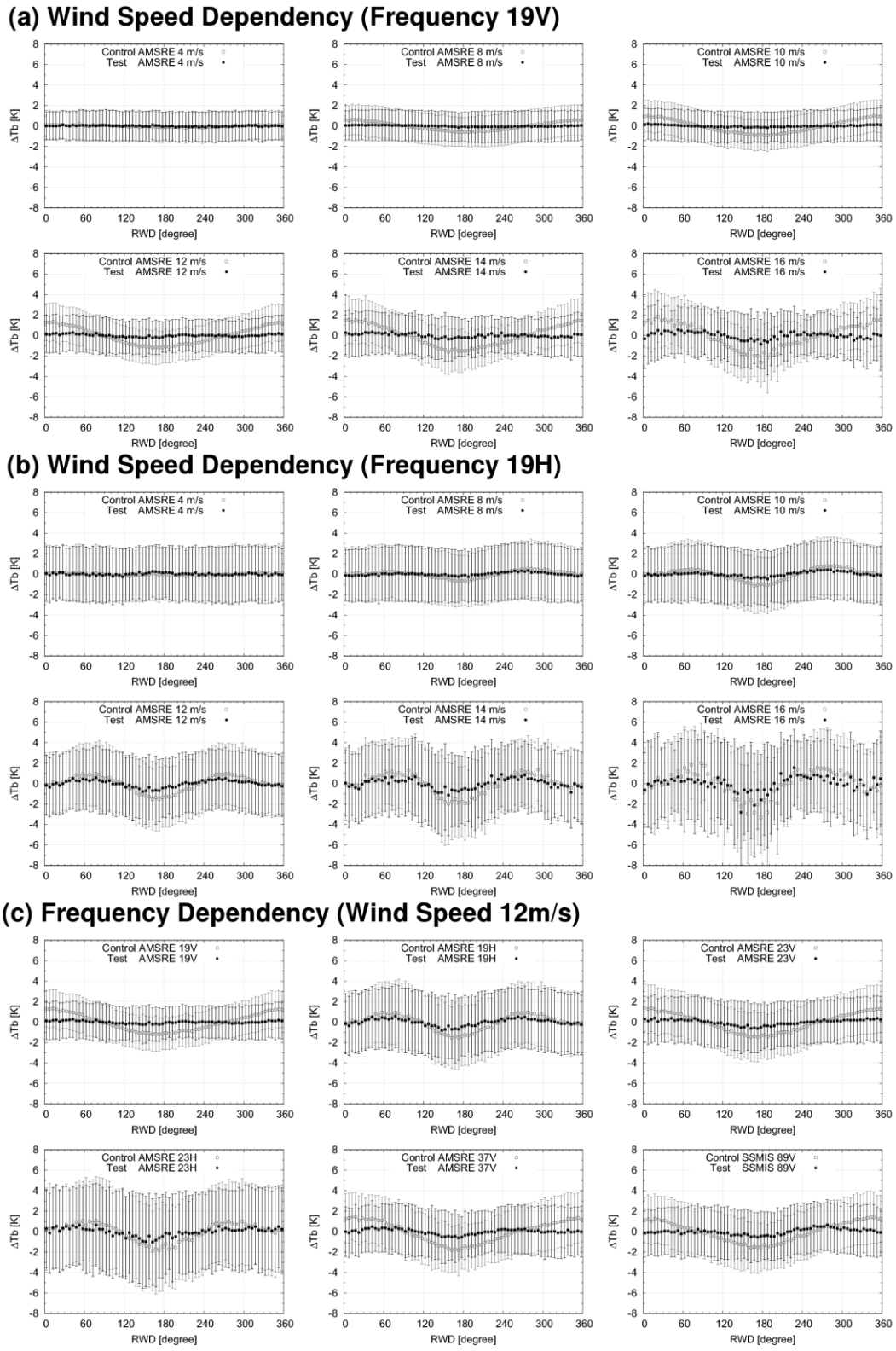

Figure 6. Comparisons of FG departure in terms of RWD between the Test run and the Control run. The biases (Test: filled circles, Control: open circles) and the standard deviations (Test: solid bars, Control: dotted bars) are displayed. (a) is AMSR-E 19V channel at 4, 8, 10, 12, 14, 16 m/s surface wind speed. (b) is same with (a) but for AMSR-E 19H channel. (c): AMSR-E for 19V, 19H, 23V, 23H, and 37V and SSMIS for 89V.

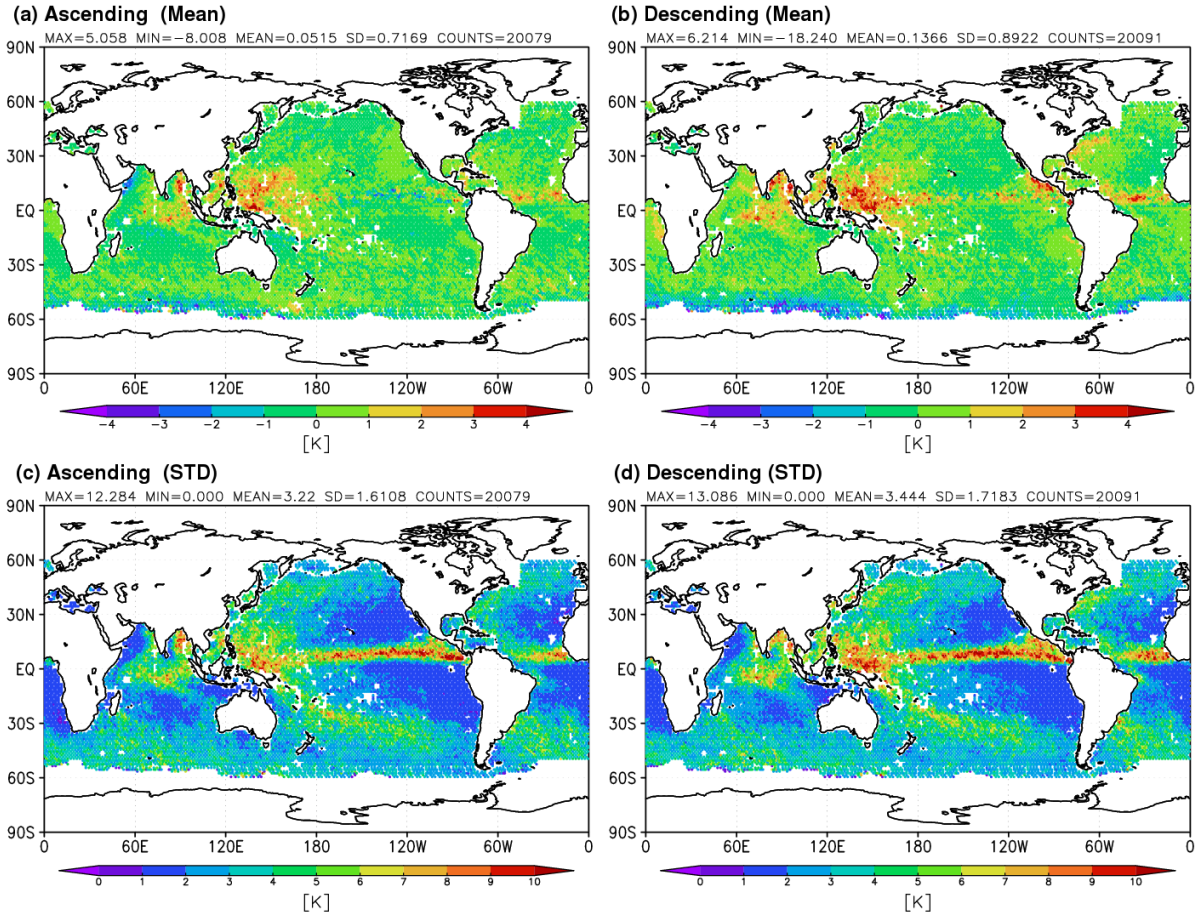

Figure 7. Mean and standard deviation of FG departure of F17 SSMIS 19V channel from the Control run in the experiment period. The ascending data are (a) mean, (c) standard deviation. The descending data are (b) mean, (d) standard deviation.

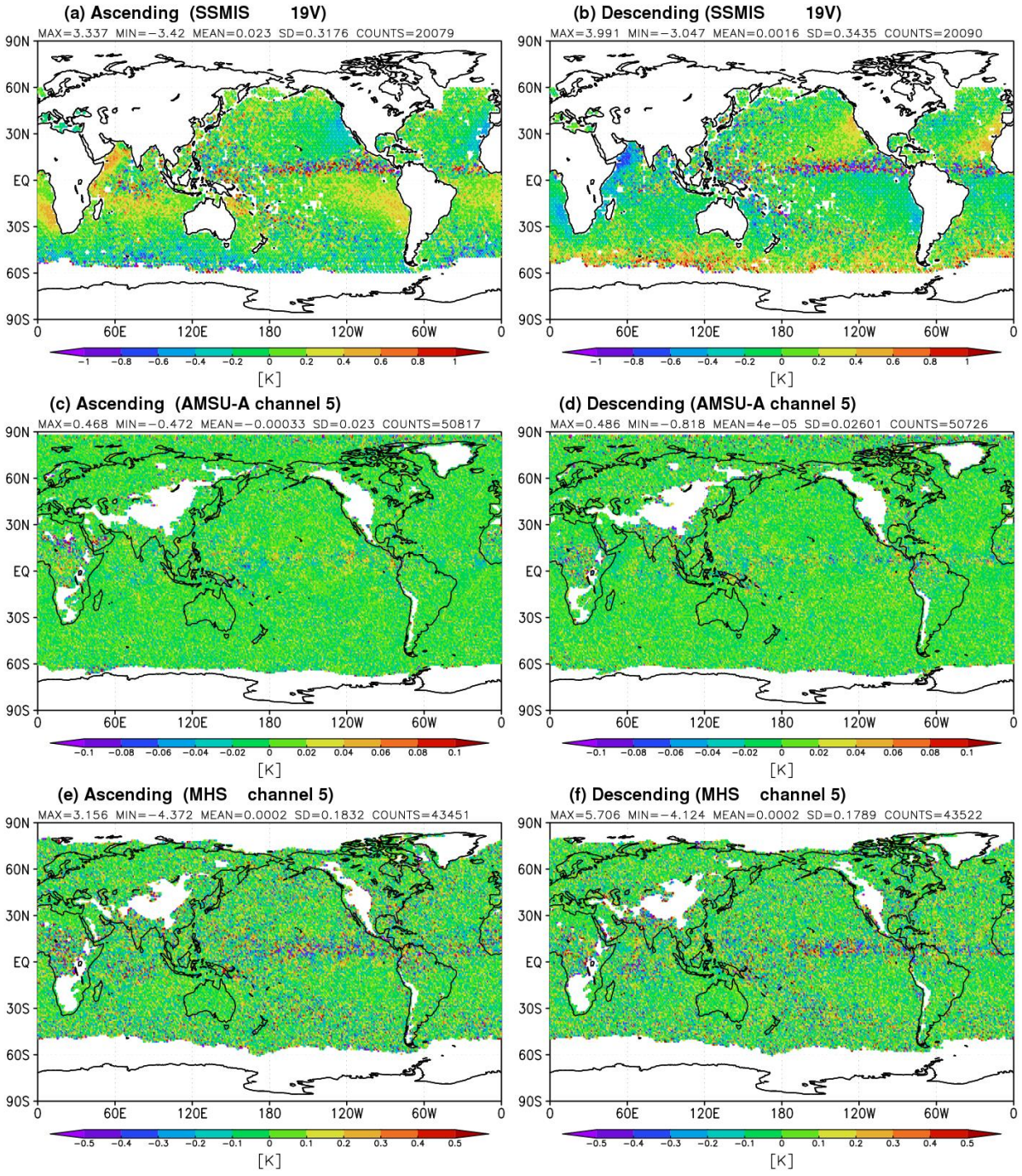

Figure 8. Mean difference of FG departure of assimilated data between the Test run and the Control run in the experiment period. (a) F17 SSMIS 19V ascending data (b) descending data, (c) Metop-A AMSU-A channel 5 ascending data (d) descending data, and (e) Metop-A MHS channel 5 ascending data (f) descending data.

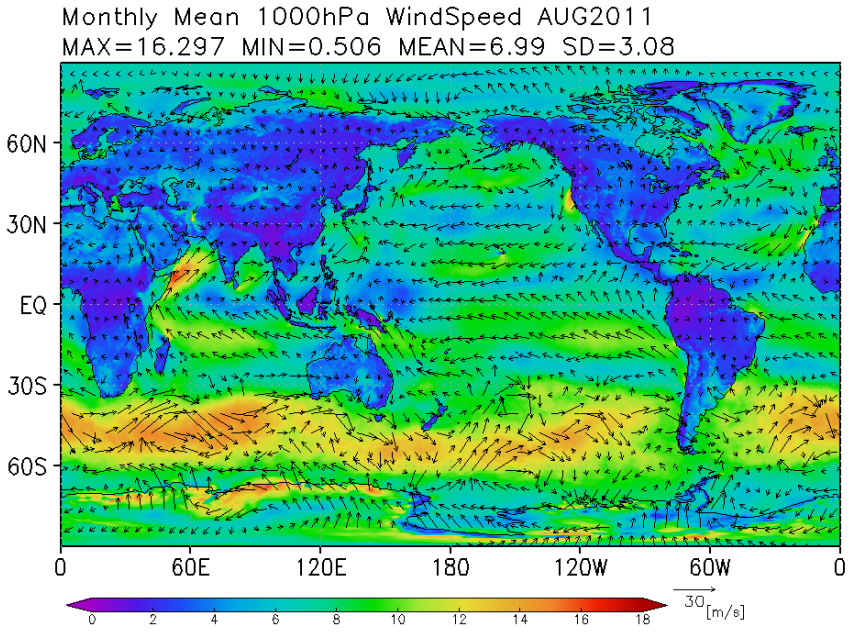

Figure 9. Monthly mean wind field at 1000 hPa for August 2011 in the Test run.

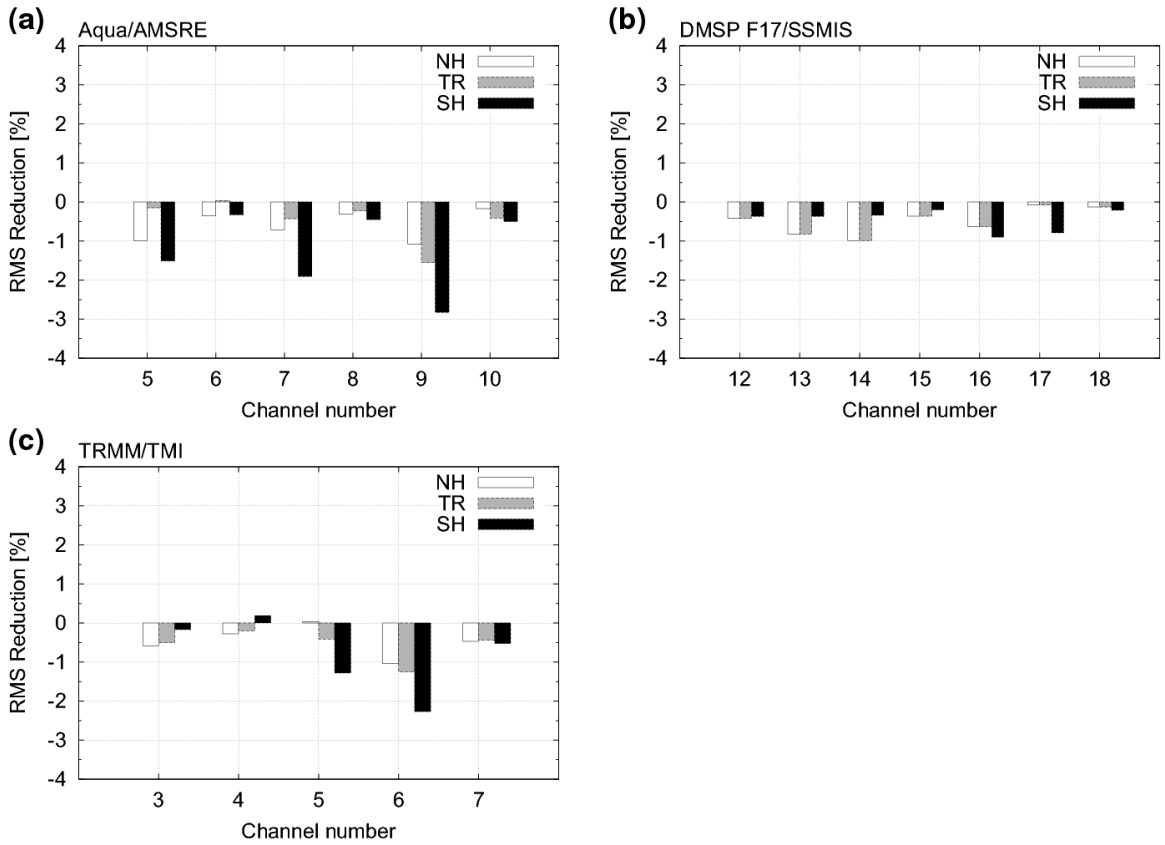

Figure 10. Standard deviation of FG departures of the microwave imagers. Standard deviation have been normalized by the value of the Control run and shown in percentage. (a) AMSR-E, (b) F17 SSMIS, and (c) TMI. White is the northern hemisphere, grey is the tropics, and black is the southern hemisphere.

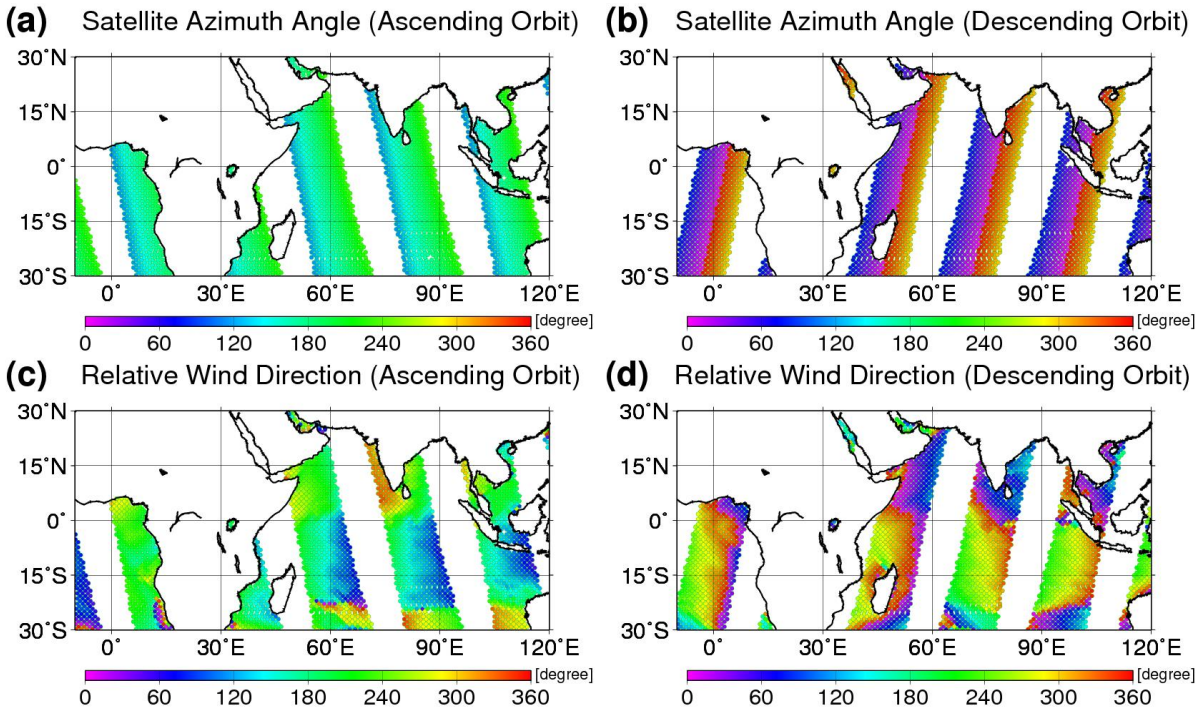

Figure 11. An example of AMSR-E satellite azimuth angle in the Arabian Sea, (a) ascending orbit, (b) descending orbit. RWD distributions are shown in (c) ascending orbit, (d) descending orbit in a single day in the experiment period. The units are in degrees. A RWD of 0 or 360 degrees corresponds to the upwind direction and 180 degree corresponds to the downwind direction.

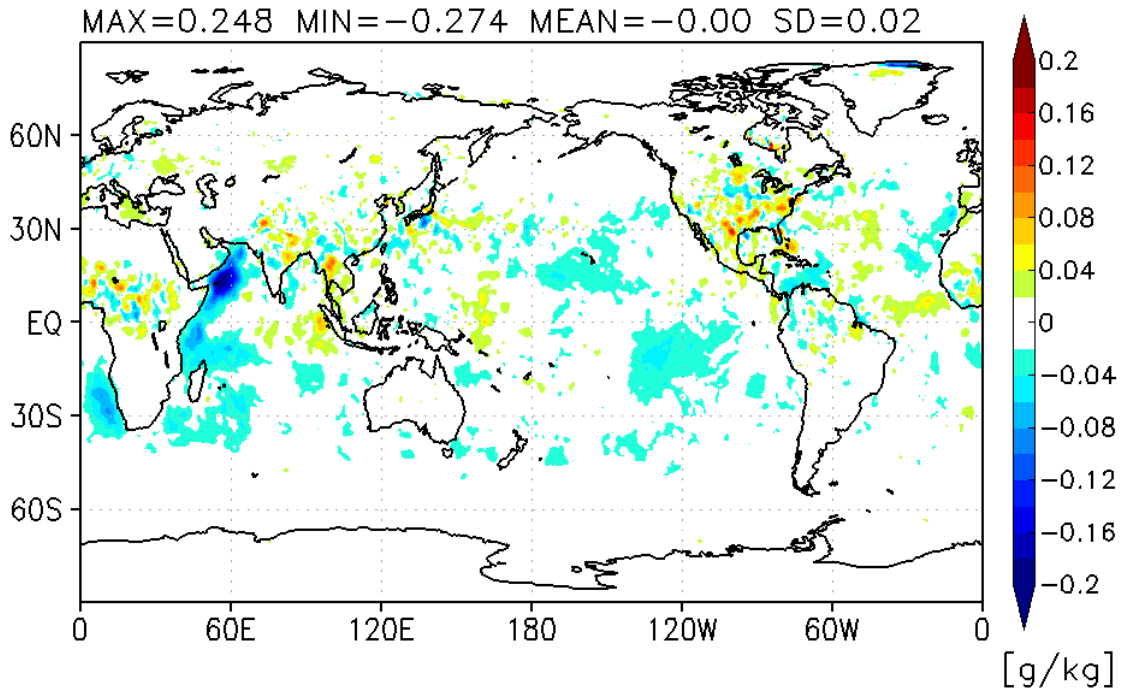

Figure 12. Mean RMS difference of 1000 hPa specific humidity analysis increment between the Test run and the Control run. Blue colours indicate a reduction in the analysis increment in the Test run. The units are in g kg^{-1}.

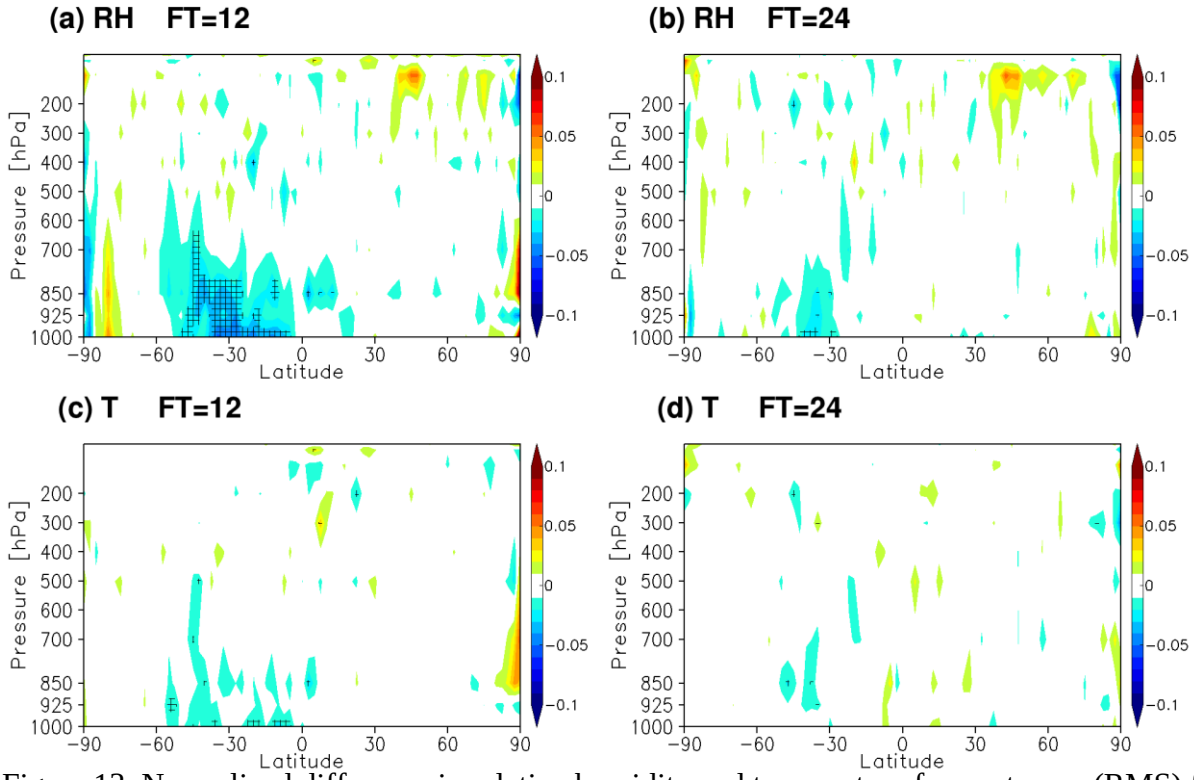

Figure 13. Normalized difference in relative humidity and temperature forecast error (RMS) for 12 hour and 24 hour forecasts. The upper panels are for relative humidity (a): 12 hour forecast, (b): 24 hour forecast. The lower panels are for temperature. Cross-hatching indicates 95% statistical significance.

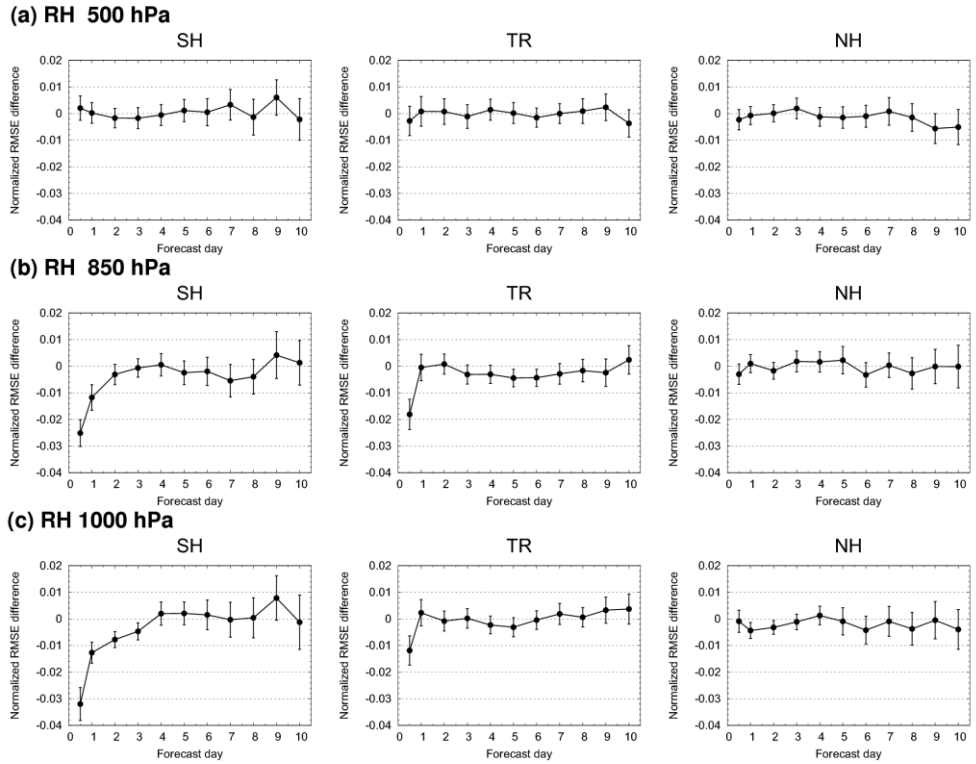

Figure 14. Normalized change in RMS forecast error in relative humidity at 500 hPa (top row), 850 hPa (middle row), and 1000 hPa (bottom row) for the southern hemisphere (latitudes -90 to -20), tropics (latitudes -20 to 20), and northern hemisphere (latitude 20 to 90). Verification is against own analysis. Scores are based on the experiment period, June 20 to October 3 2011. Error bars indicate the 95% confidence level.

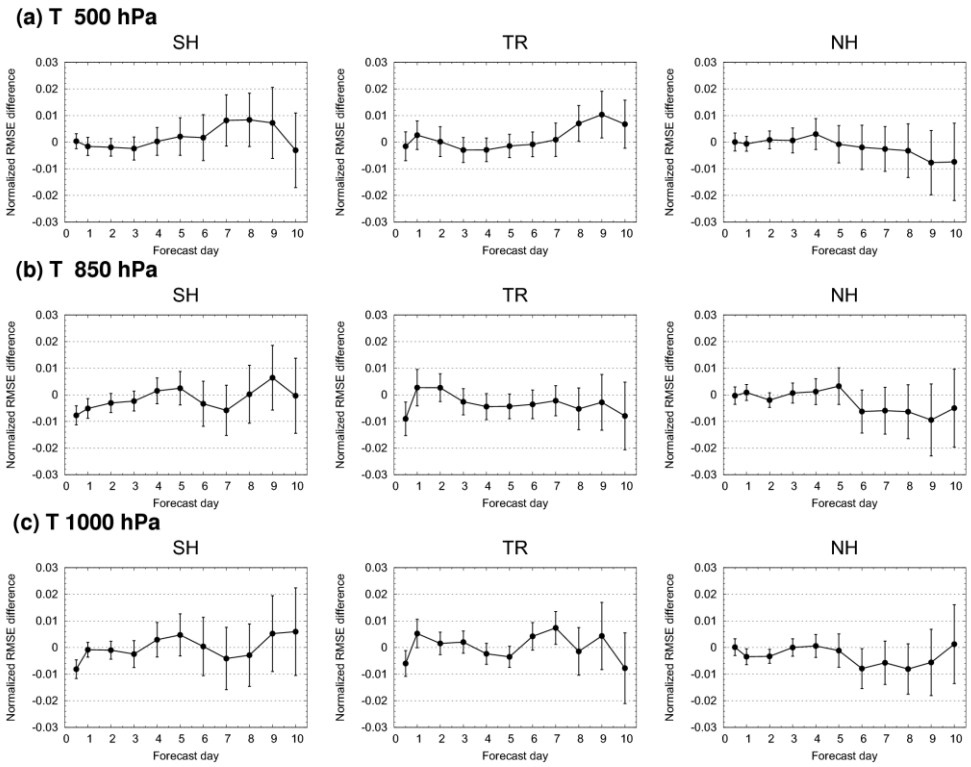

Figure 15. Same as Figure 14 but for temperature.

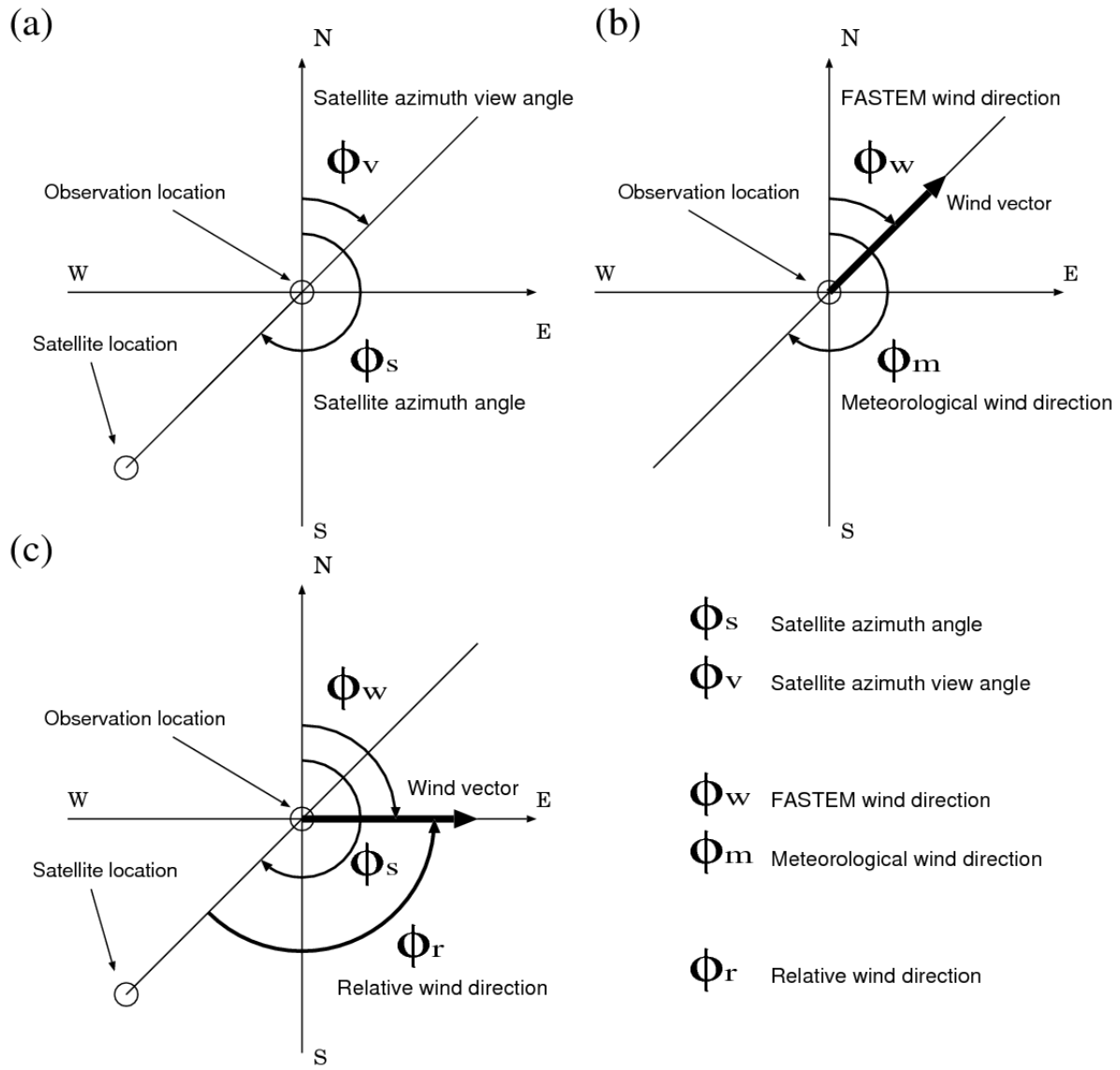

Figure 16. Definitions of angles. (a): Satellite azimuth view angle and Satellite azimuth angle. (b): FASTEM wind direction and Meteorological wind direction. (c): Relative wind direction (westerly wind case). Wind vector is drawn in thick black arrow.